InSAR time-series
A quick introduction

Piyush Agram
Jet Propulsion Laboratory

Jun 29, 2015
@UNAVCO

Thanks to my colleagues from JPL, Caltech, Stanford University and from all over the world for images and material used in this talk.

Overview

- Radar interferometry
  - Introduction to InSAR
  - Error sources and limitations
  - Motivation for time-series InSAR

- Time-series InSAR
  - Persistent Scatterer (PS) Techniques
  - Small Baseline (SB) Techniques
  - Hybrid Techniques
  - Challenges

Radar interferometry

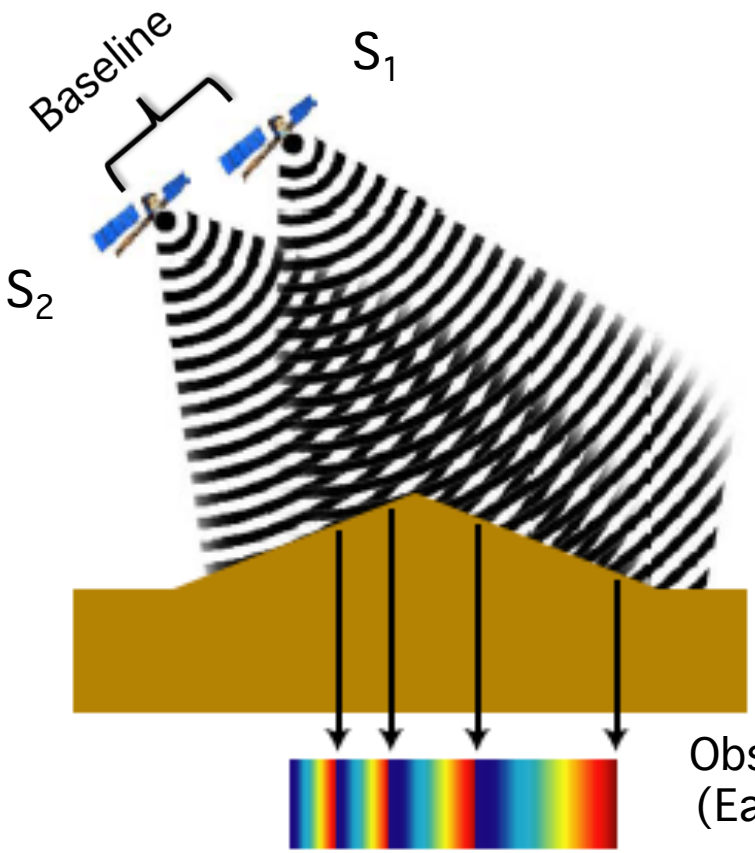

Phase pattern modulated by topography

(Sang-Ho Yun, 2008)

$$\left(\frac{A_1}{|\vec{r_1}|^4}\cdot e^{-jk|\vec{r_1}|}\right)\times \text{conj}\left(\frac{A_2}{|\vec{r_2}|^4}\cdot e^{-jk|\vec{r_2}|}\right)$$

$$\phi_{ifg} = -\frac{4\pi}{\lambda}\cdot(|\vec{r_1}| - |\vec{r_2}|)$$

SAR images represent precise observations of radar echo Amplitude and Phase.

Global Height Mapping – Tandem Imaging

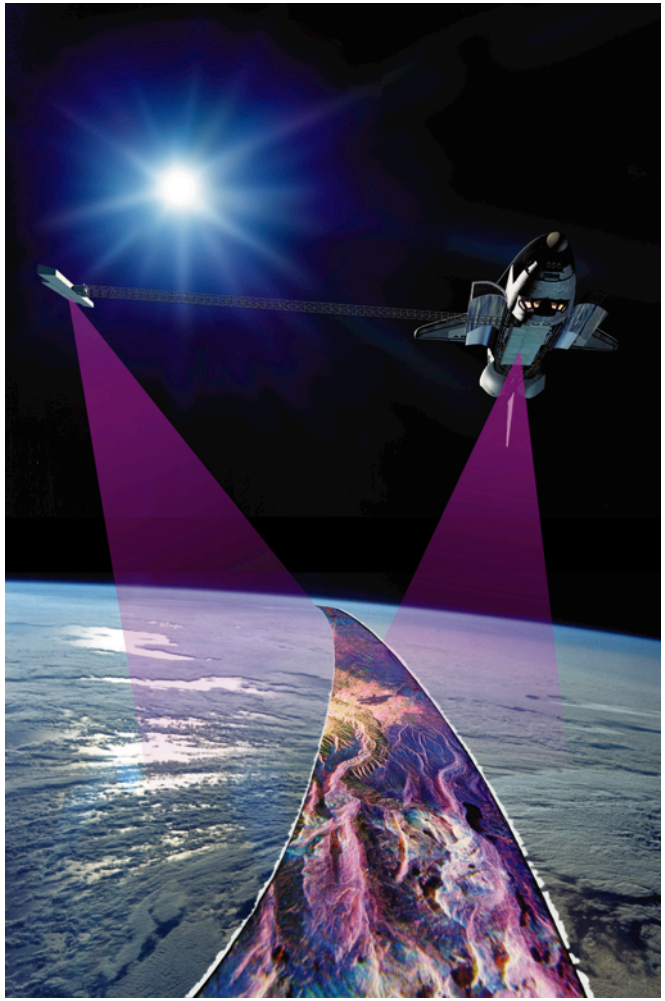

Image: NASA/ JPL-Caltech

(Left) SRTM and (Right) Tandem-X

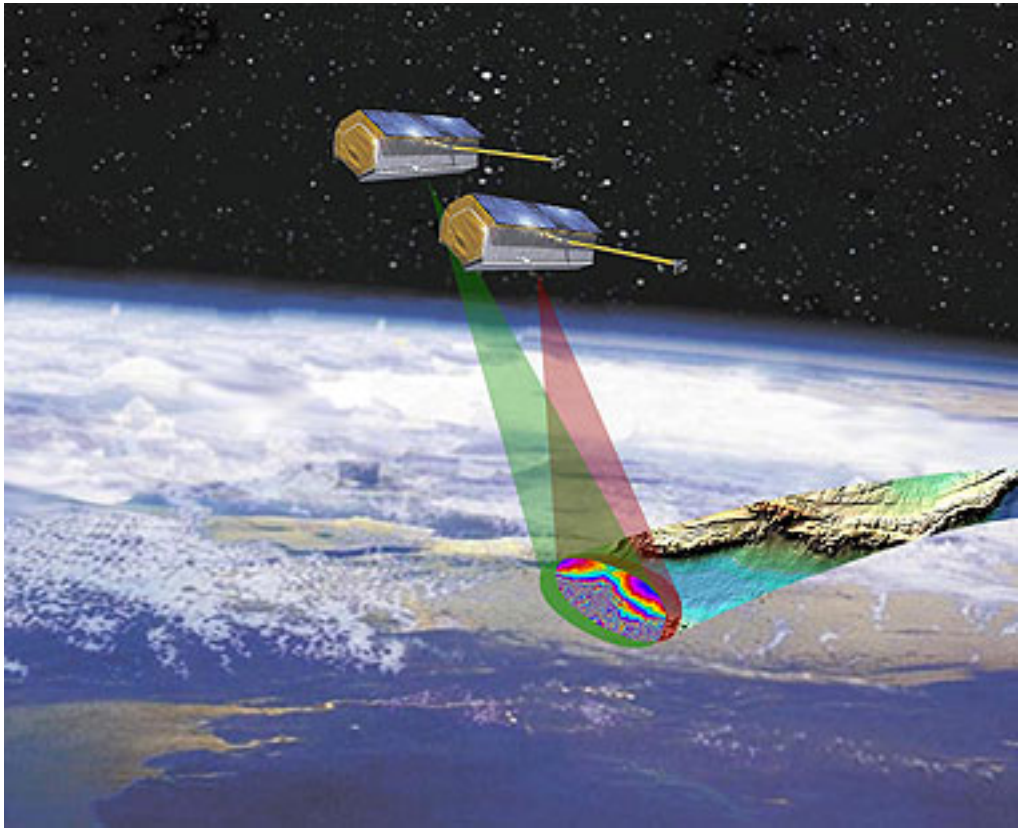

Image: EADS Astrium

Repeat-pass Interferometry

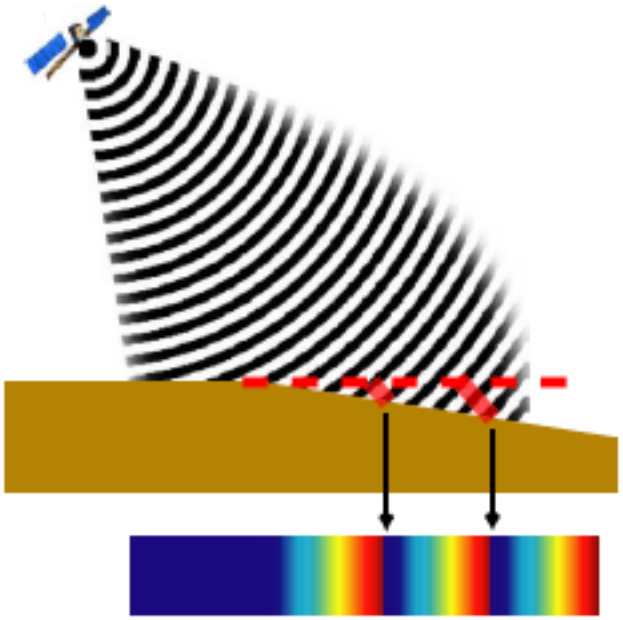

Surface could have deformed between acquisitions

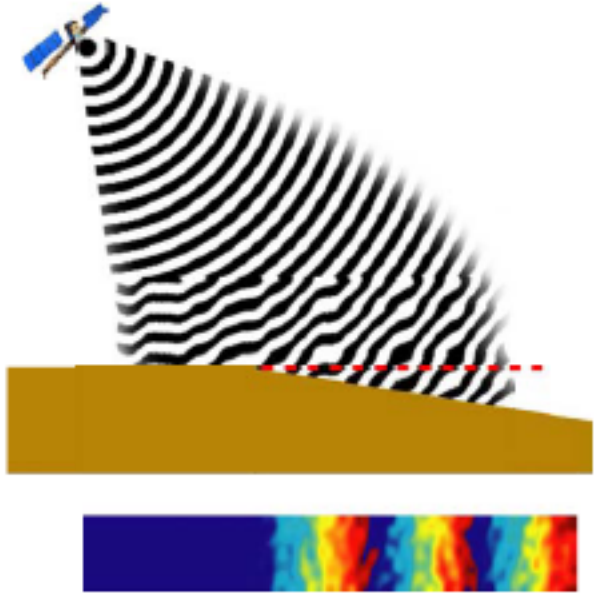

Atmospheric properties could be significantly different between acquisitions

(Sang-Ho Yun, 2008)

Typical InSAR / D-InSAR workflow

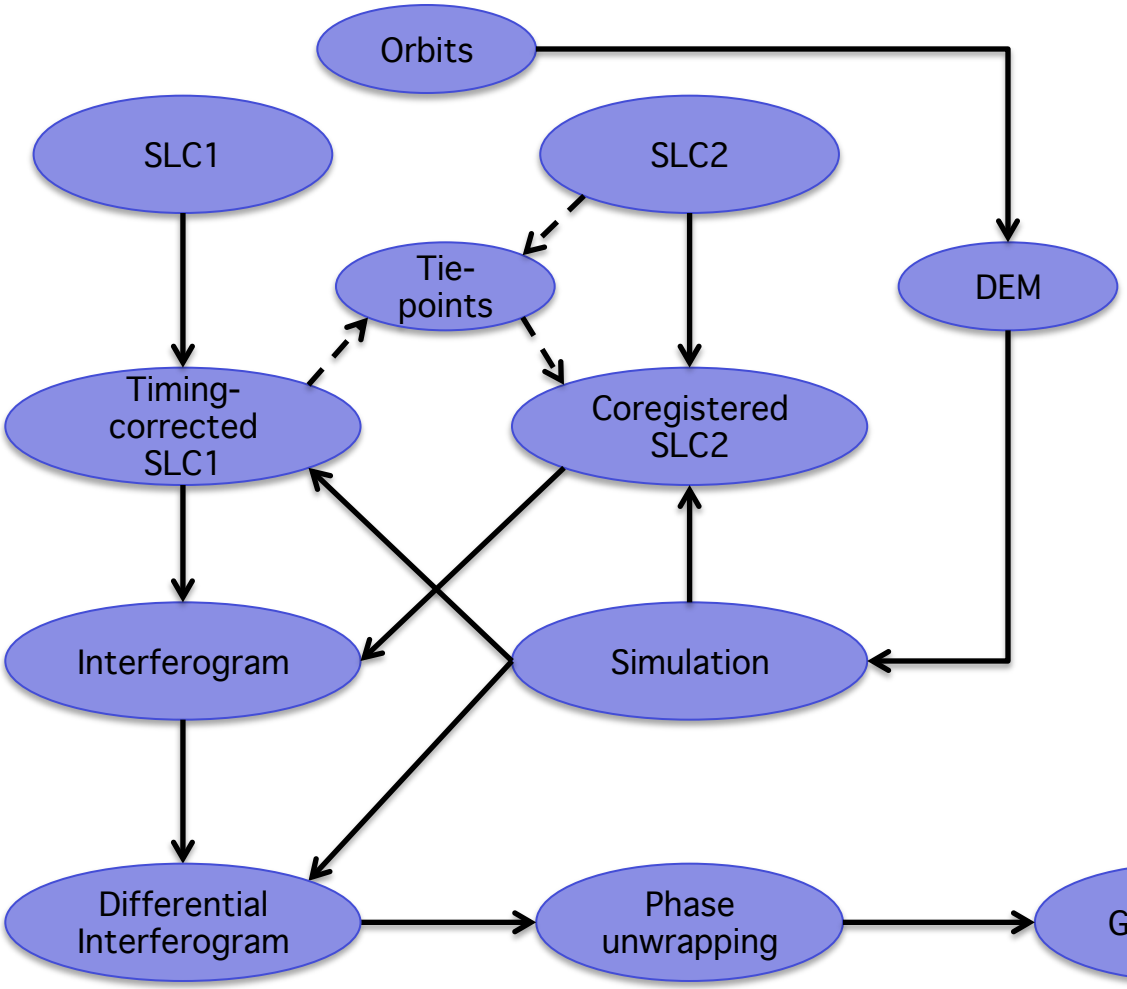

- Most modern day sensors provide precise orbit information to within 10 cm.
- Timing errors result in constant translation between master and coregistered SLC.
- In absence of reliable orbits, one can use traditional approach of amplitude coregistration.

Differential Interferometry

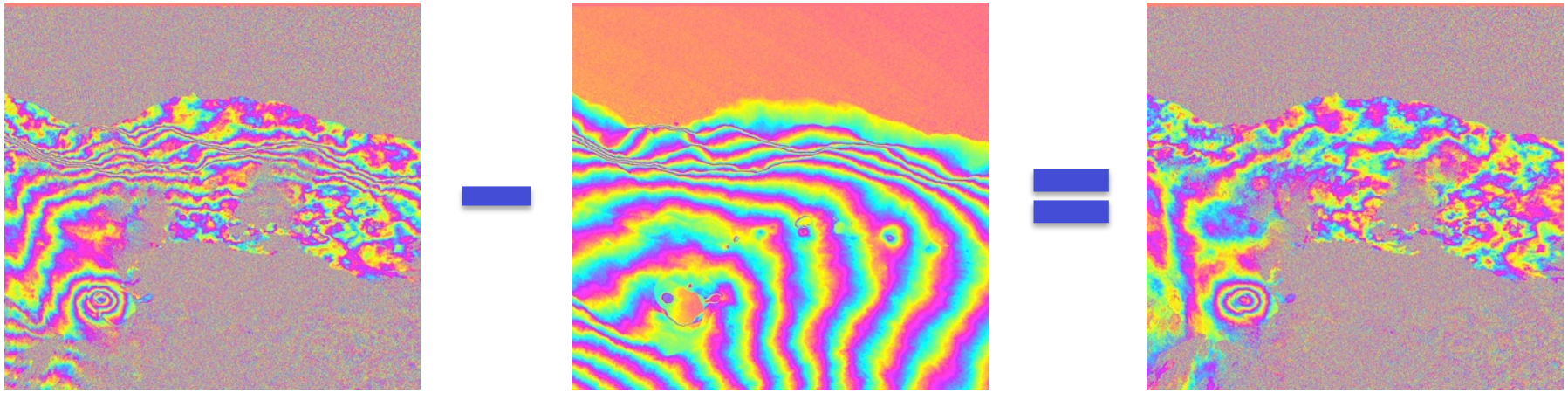

Interferogram with earth's curvature removed

Simulation using the SRTM DEM

Flattened interferogram with topography removed

- What are the noisy regions in the differential interferogram?
  - Decorrelation
- Can all the phase in the differential interferogram be attributed to surface deformation?
  - Atmosphere

Decorrelation

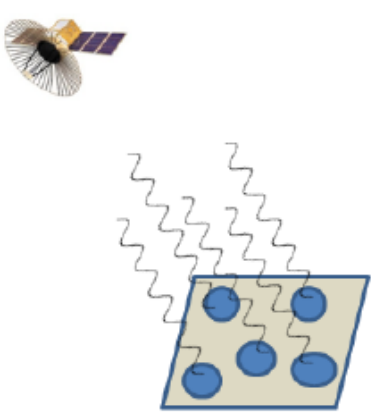

Observed Signal = sum of returns from scatterers.

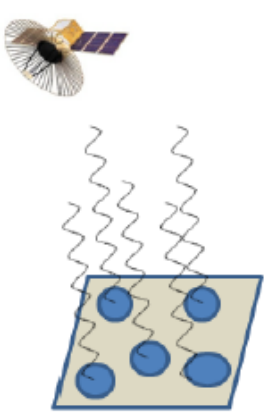

Change in look angle.

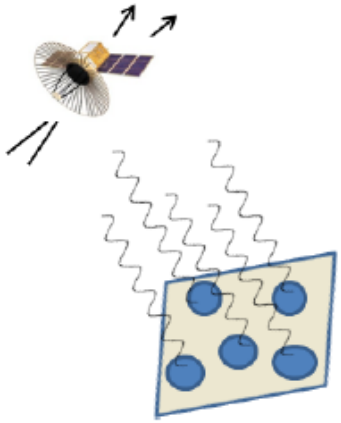

Non-parallel orbits.

Geometric decorrelation

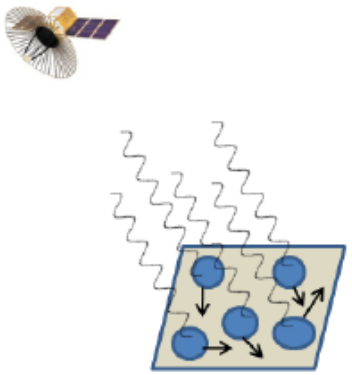

Random motion of scatterers (or) Change in scattering properties.

Temporal decorrelation

Baseline and decorrelation

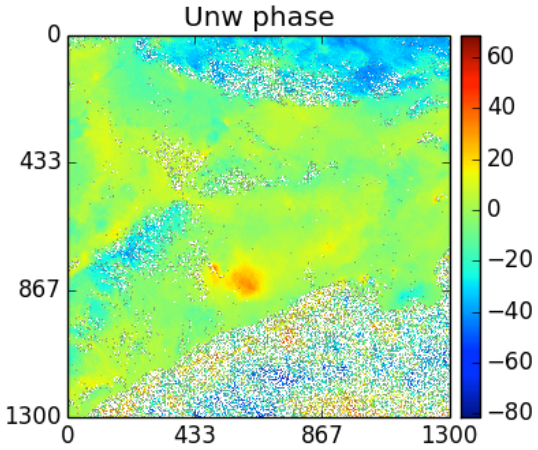

Bperp = 2m, Δt=1yr

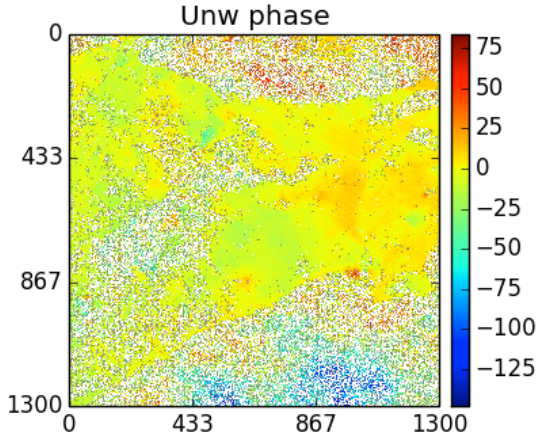

Bperp = 400m, Δt=1yr

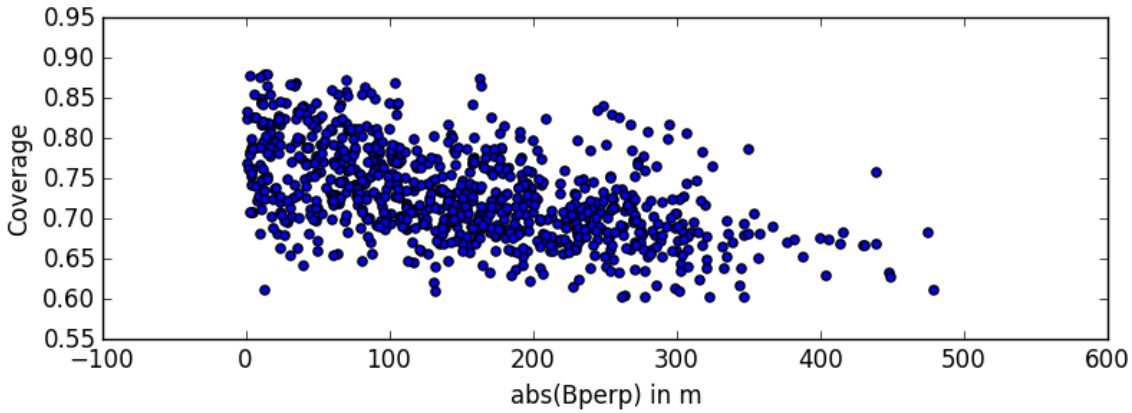

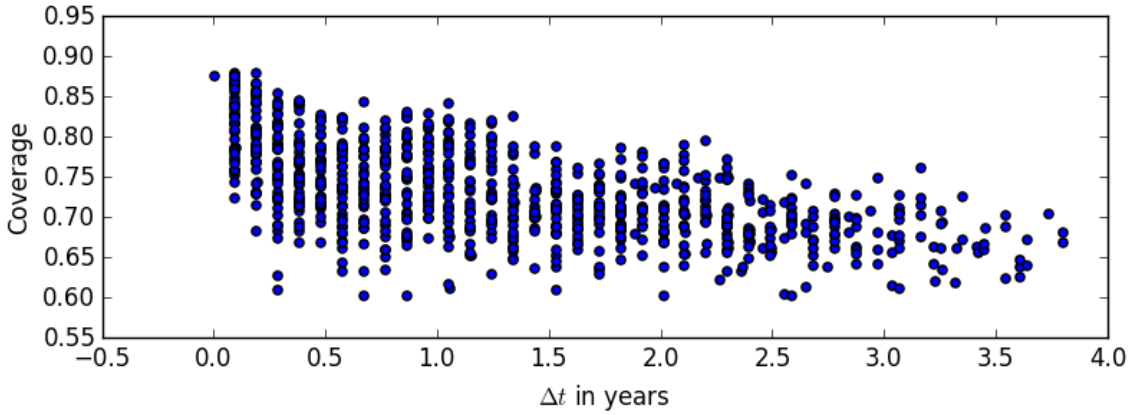

881 ERS + Envisat interferograms over Los Angeles, California
Fraction of image with coherence > 0.4

Scattering properties change with time

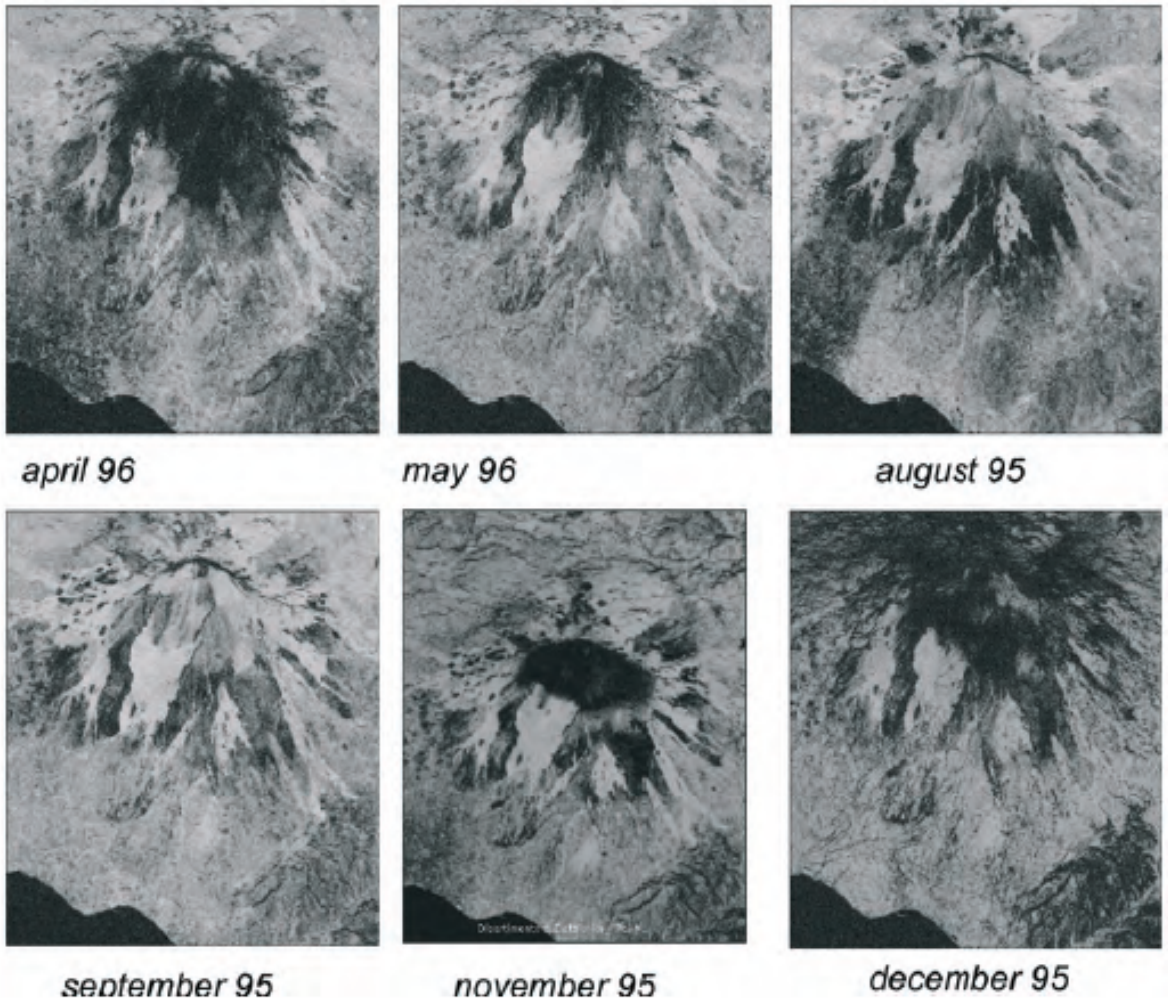

Image: ESA

Figure 1-2: Tandem coherence of Mount Etna in different seasons

Impact of wavelength on SAR images

EM waves interact most strongly with objects on the size of the wavelength

L (24 cm) C (6 cm) X (3 cm)

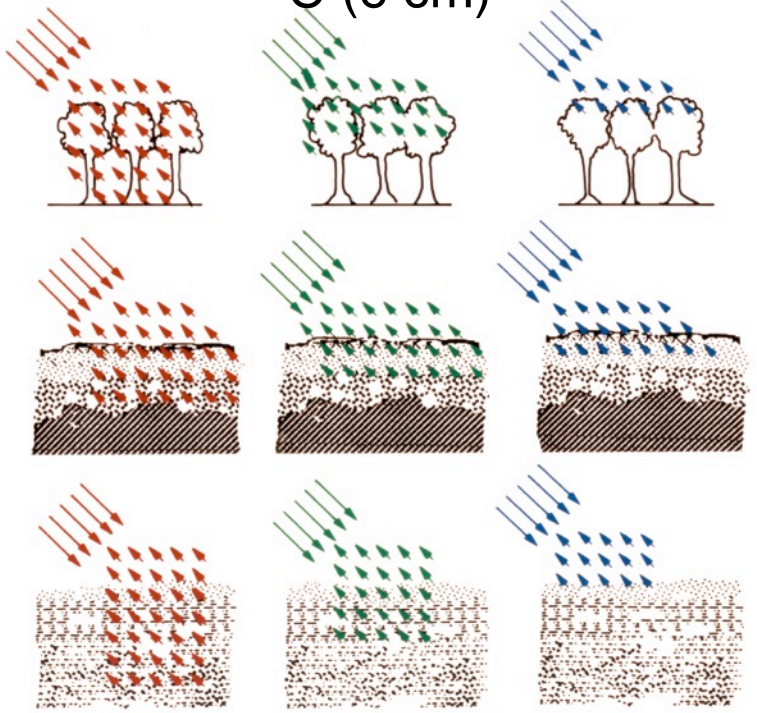

Forest: Leaves reflect X-band wavelengths but not L-band

Dry soils: Surface looks rough to X-band but not L-band

Ice: Surface and layering look rough to X-band but not L-band

From: Rosen (2014)

Impact of wavelength on InSAR

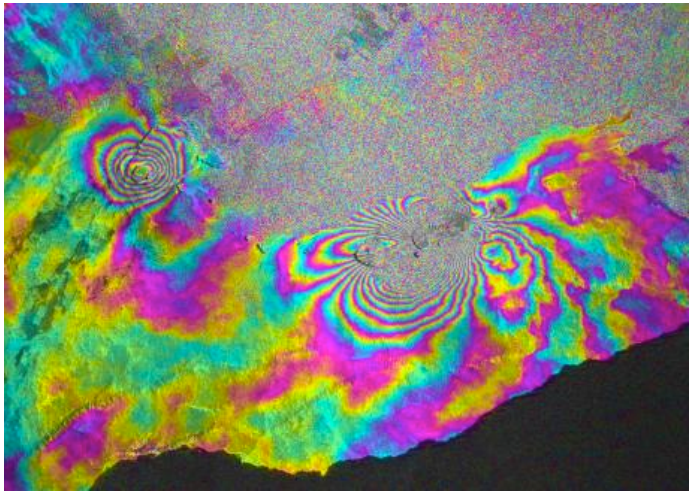

Image: NASA/JPL-Caltech

Kilauea Volcano, Hawaii
(24-days, X-band)

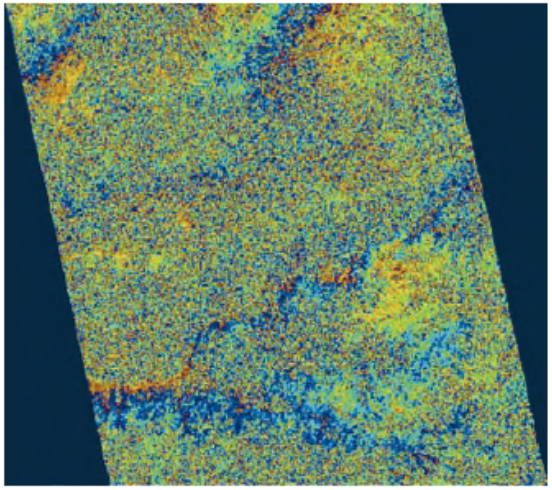

Image: ESA

Latur, Maharashtra
(8 months, C-band)

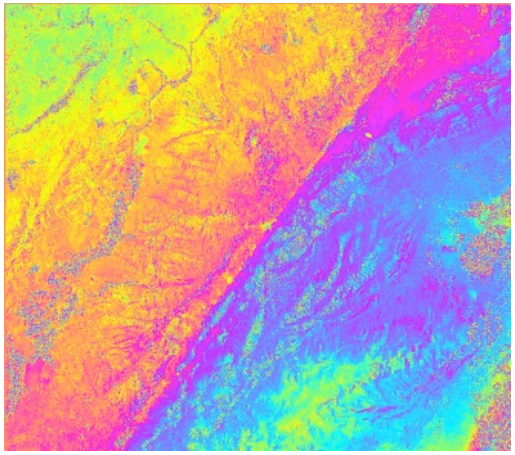

Parkfield, California
(3 years, L-band)

Temporal decorrelation effects depend on terrain type but in general decrease with increasing wavelength.

Stratified troposphere

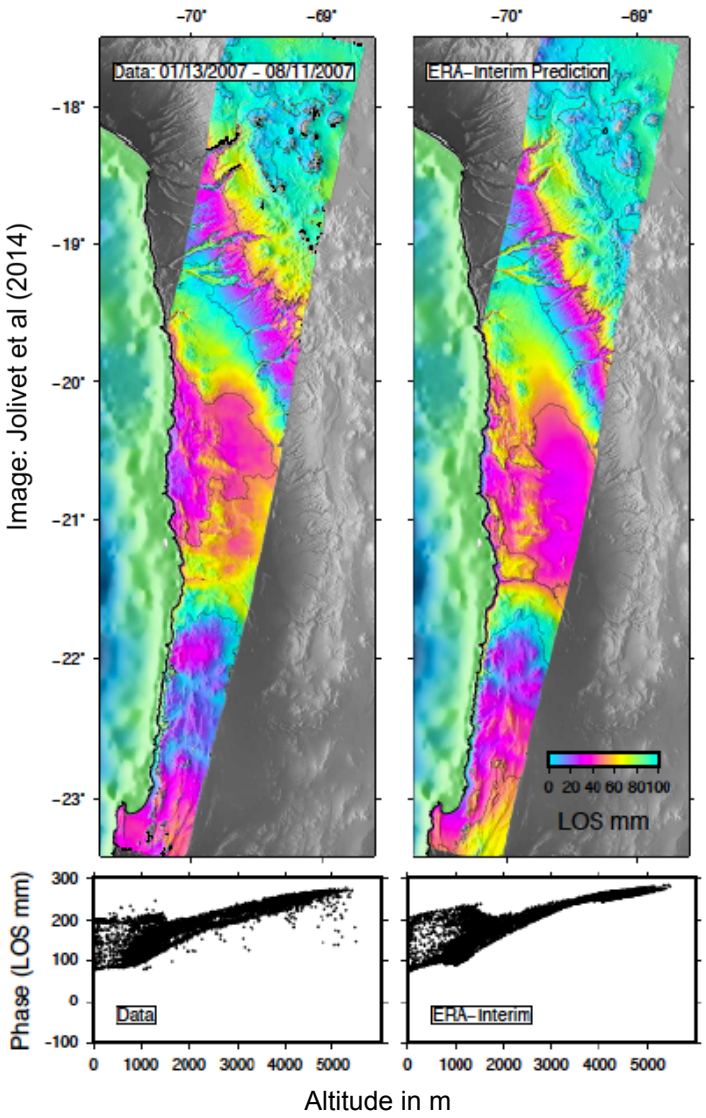

Image: Jolivet et al (2014)

- Path delay depends on altitude of point being imaged due to the stratification of the troposphere
- Active area of research
- Long wavelength effects can be reasonably well captured by weather models
- Ability to correct is driven by the resolution of global weather models – both temporal and spatial.

Tropospheric turbulence

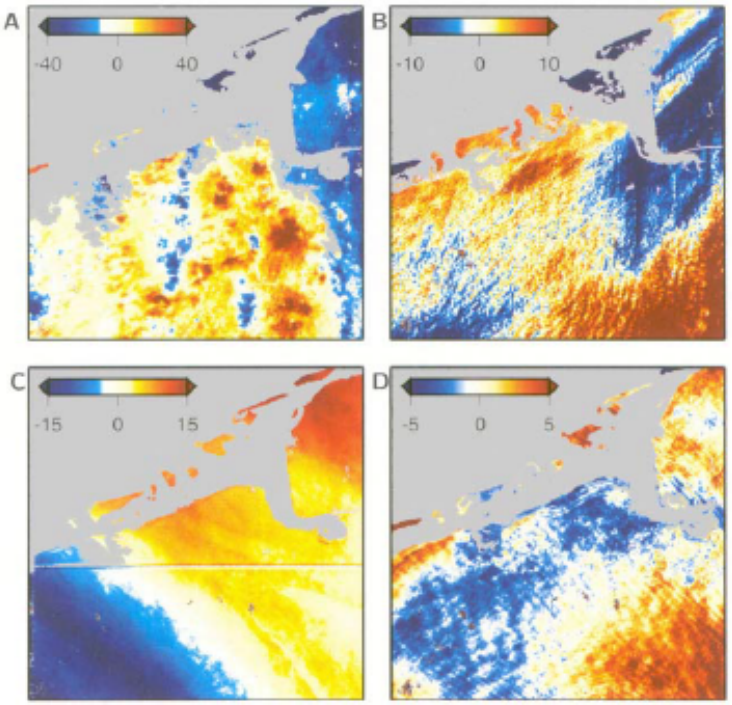

Fig. 4.31. Eight differential tandem interferograms over the northern part of the Netherlands (100 × 100 km), showing only atmospheric signal, expressed in millimeters zenith delay. Note the different ranges in the color scales. **(A)** Jul 1995, **(B)** Aug 1995, **(C)** Dec 1995, **(D)** Mar 1996.

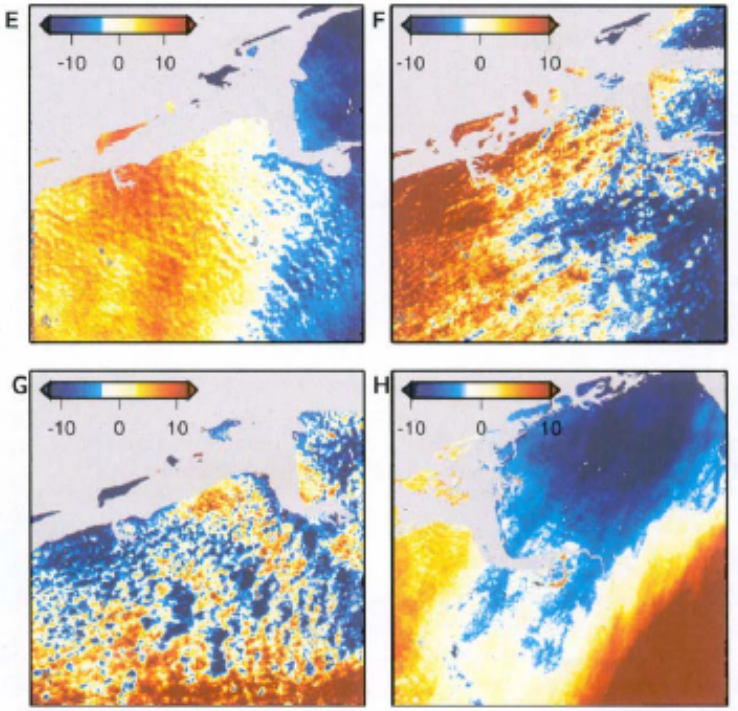

Fig. 4.31.—*continued* **(E)** Apr 1996, **(F)** May 1996, **(G)** Aug 1996, **(H)** Feb 1996.

Image: Ramon Hanssen (2003)

- High spatial frequency phase artifacts
- Not captured by low resolution weather models or sparse GPS networks

Ionosphere – polar regions

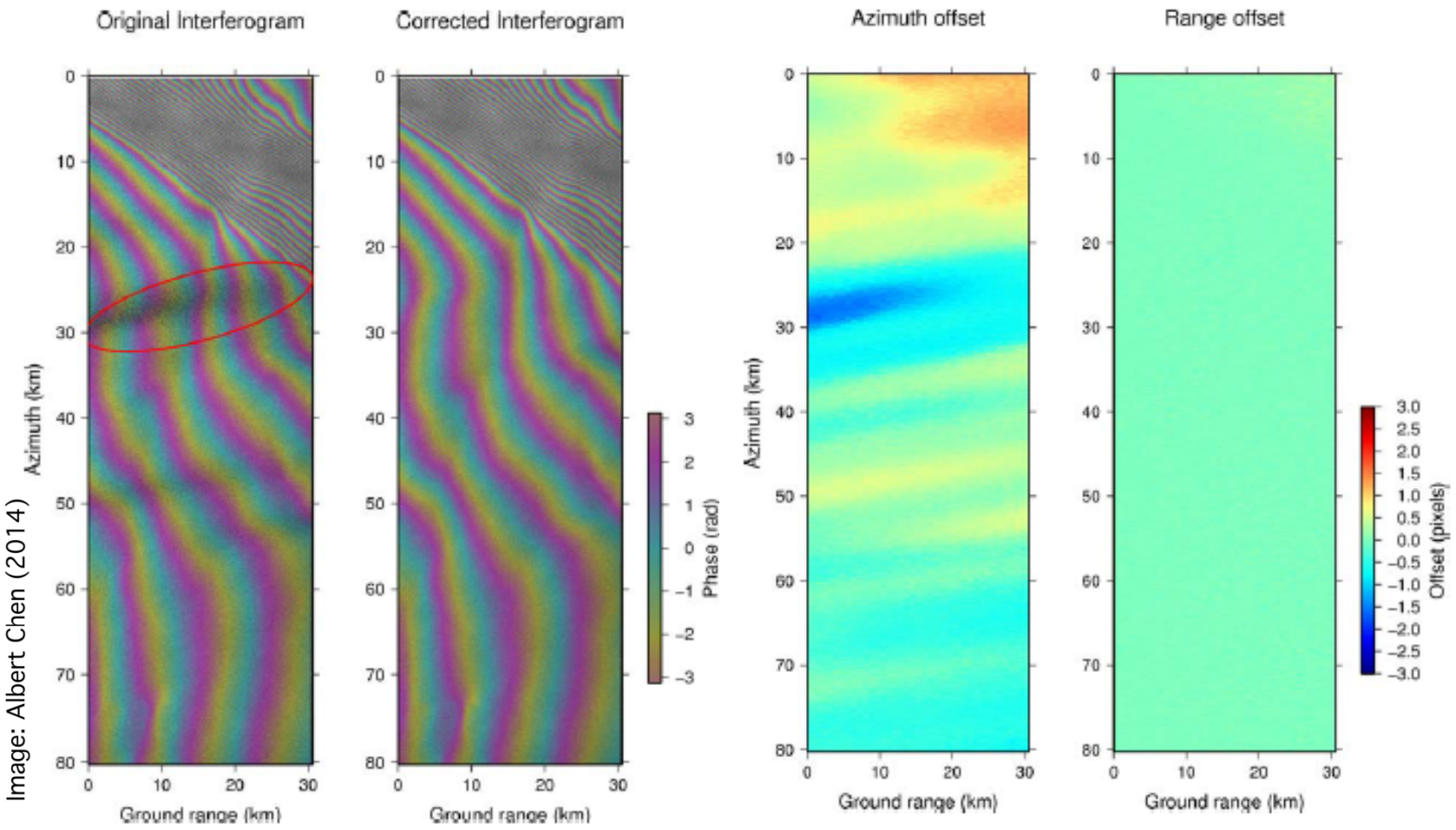

Image: Albert Chen (2014)

Effects are wavelength dependent and can be reasonably corrected using split-band processing.

Ionosphere – equatorial regions

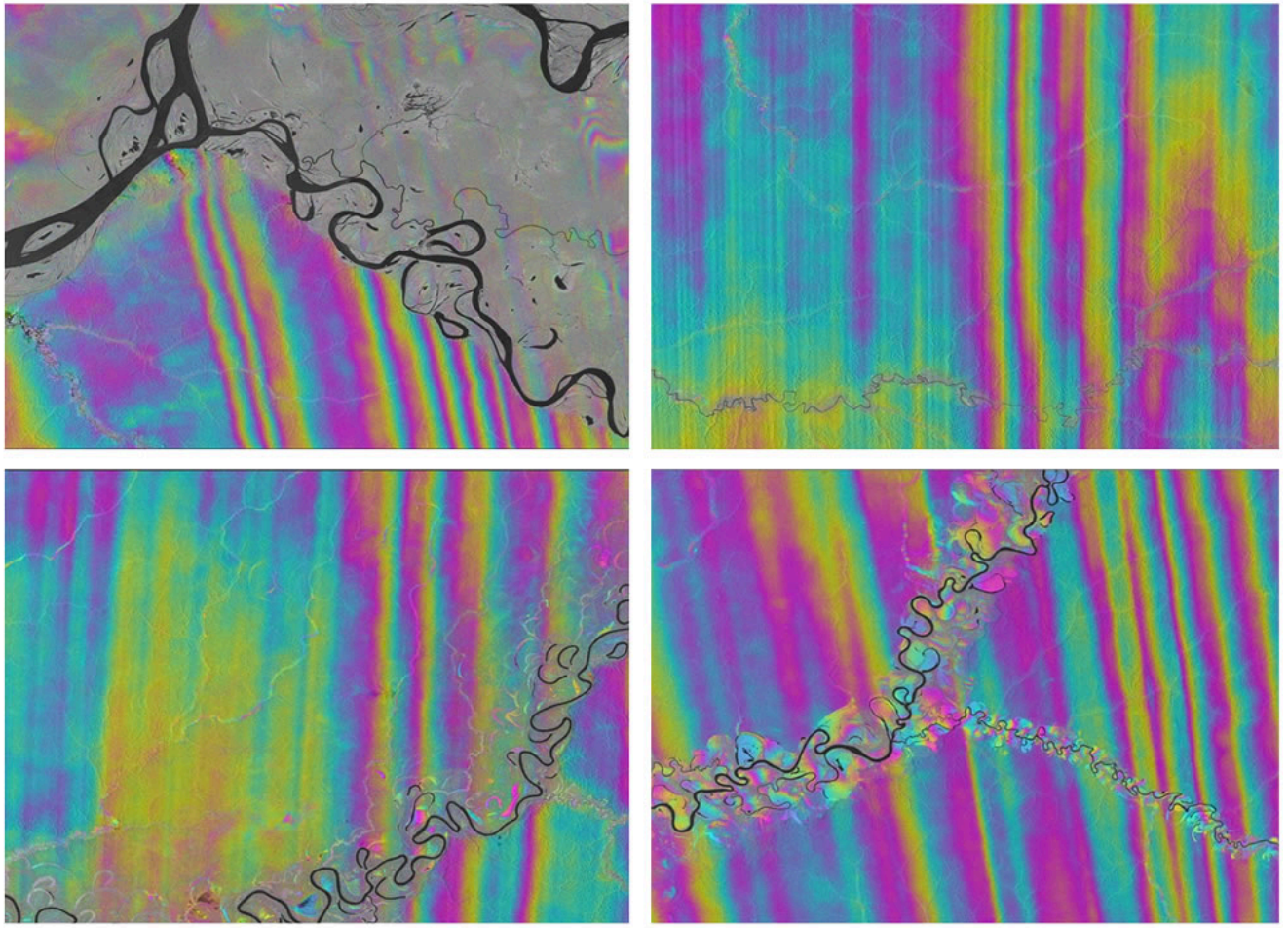

Image: Franz Meyer (UAF)

Ionospheric Signals in L-band InSAR Data near the Equator

Phase unwrapping

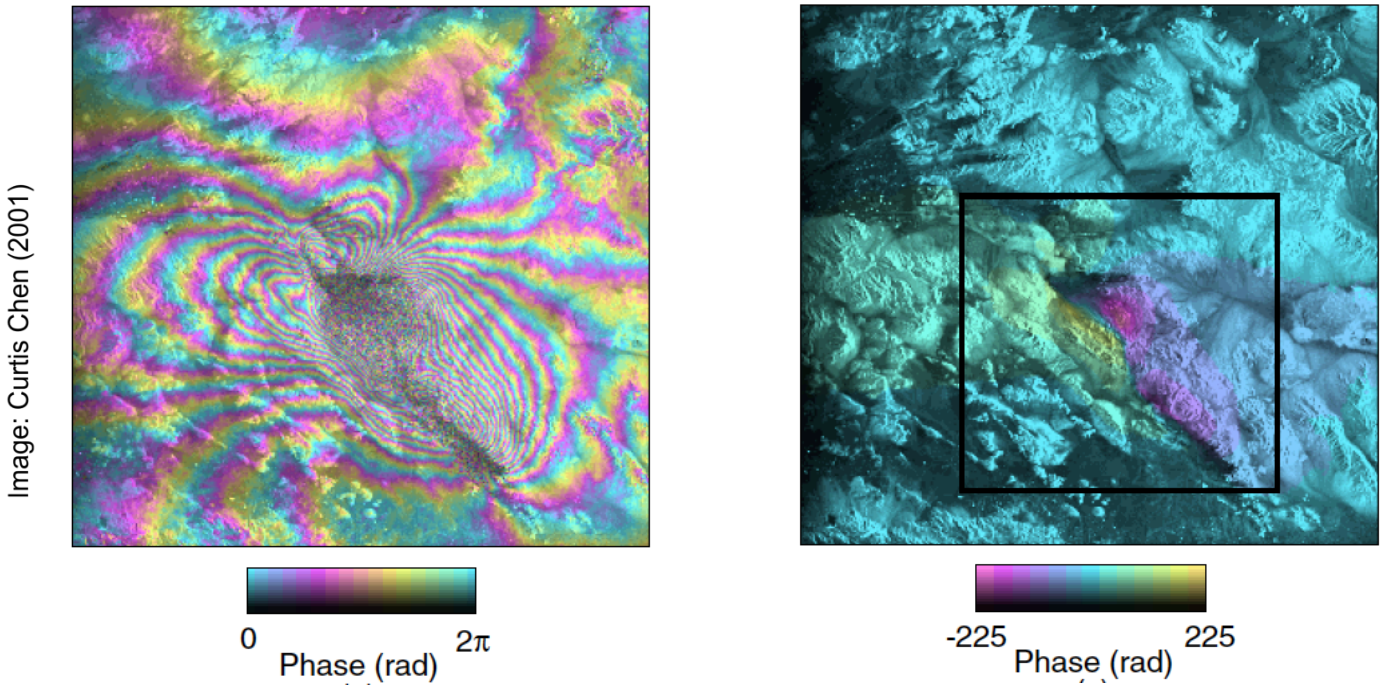

$$\psi(i,j) = \phi(i,j) + 2\pi N(i,j)$$

- An integer number of cycles added to every pixel
- First subjective operative in the workflow

Different methods produce different solutions

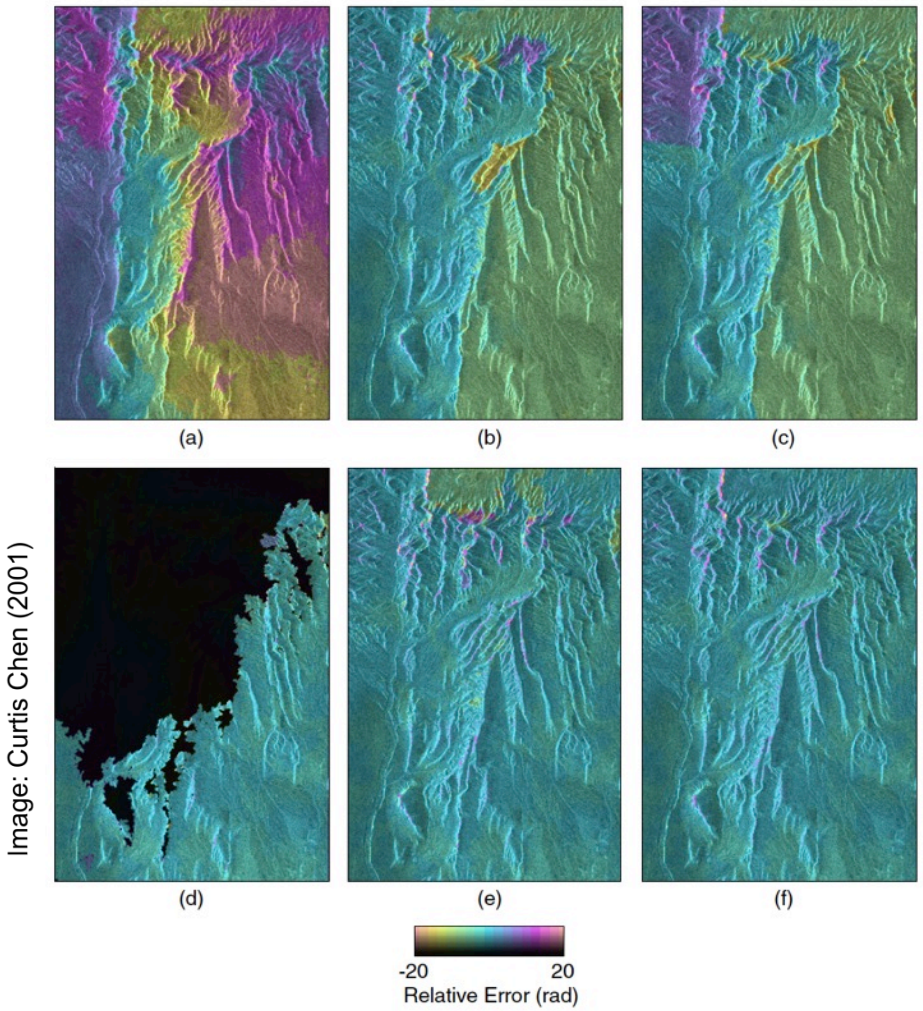

Image: Curtis Chen (2001)

Figure 7.4 Relative unwrapped-phase errors for the Death Valley test data from different algorithms: (a) least-squares; (b) MCF; (c) LPN; (d) residue-cut; (e) MST; (f) SNAPHU. The interferogram magnitude is shown in gray-scale brightness. Black areas in (d) indicate that no solution was produced.

Without ground control points or a very reliable deformation model, detecting unwrapping errors is very hard.

Decorrelation and connected components

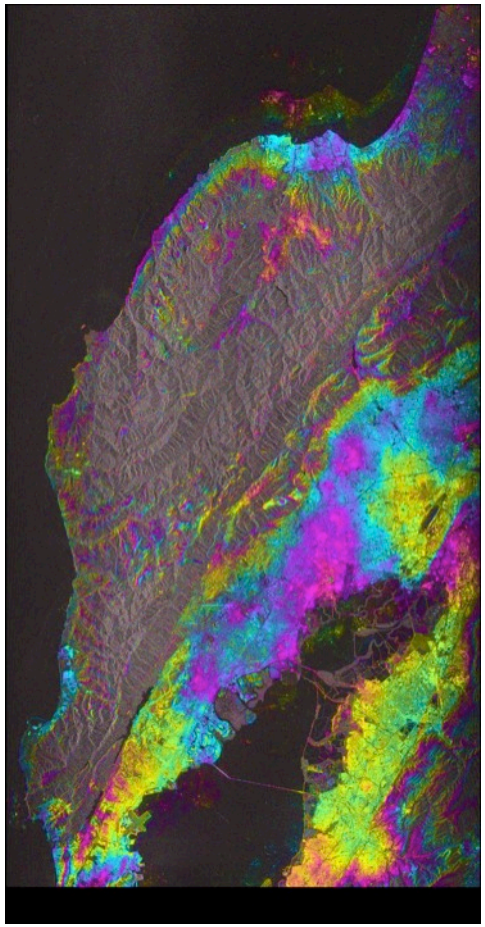

Wrapped Interferogram

-π  π

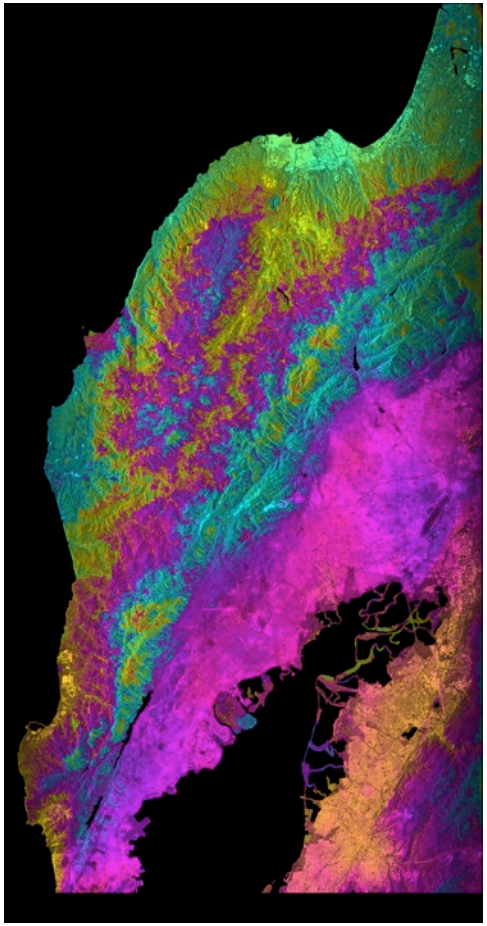

Unwrapped Interferogram

-12.5  12.5

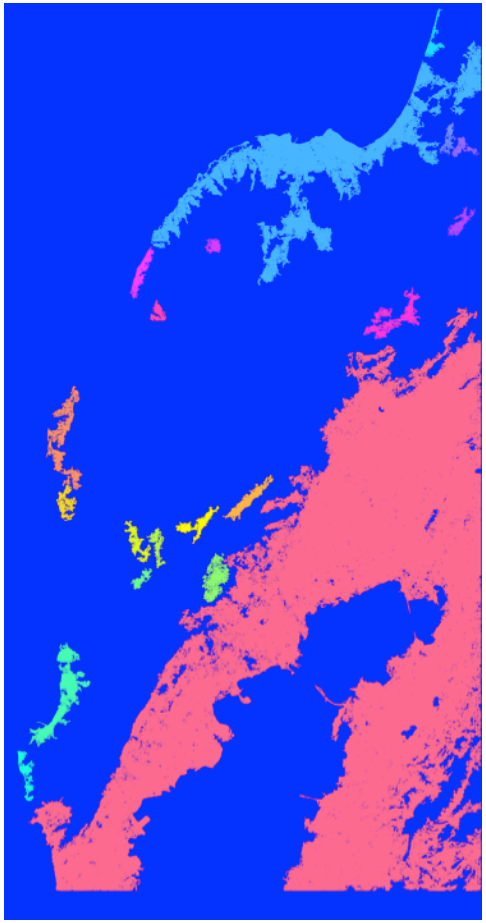

Connected components (Self-consistent unwrapped regions)

D-InSAR Phase Analysis

$$\phi_{ifg} = [\phi_{defo} + \phi_{tropo} + \phi_{iono} + \phi_{dem} + \phi_{base} + \phi_{noise}]_{2\pi}$$

- Differences in atmospheric conditions between two acquisitions
  - Tropospheric path delay affects all microwave frequency
  - Ionospheric path delay depends on imaging wavelength
- Errors in imaging geometry
  - Orbit errors
  - DEM errors
  - Timing errors
- Differences in scattering properties of the target
  - Geometric decorrelation
  - Temporal decorrelation
- Unmodeled systematic effects
  - Soil moisture / moisture content of vegetation
  - Earth tides

D-InSAR Error Budget (NISAR model)

$$\phi_{ifg} = [\phi_{defo} + \phi_{tropo} + \phi_{iono} + \phi_{dem} + \phi_{base} + \phi_{noise}]_{2\pi}$$

	L-band	
	Bhuj	Barstow
Troposphere	37.3mm	20.1mm
Ionosphere	0.5mm	0.5mm
DEM Error	Can be mitigated with filtering	
Baseline Error	Negligible	
Decorrelation	3.2mm	2.5mm
Total (RMS)	37.5mm	20.2mm

Northern Summer Period. 100m resolution. 100m Baseline. Two points 50kms apart. 12-day ascending pair.

Applications of D-InSAR

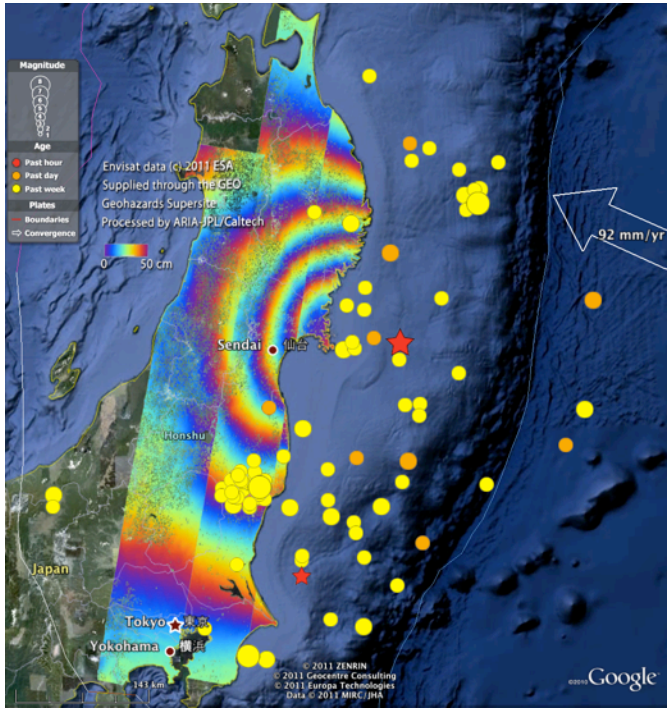

Tohoku Oki EQ (2011) processed by the ARIA project at JPL

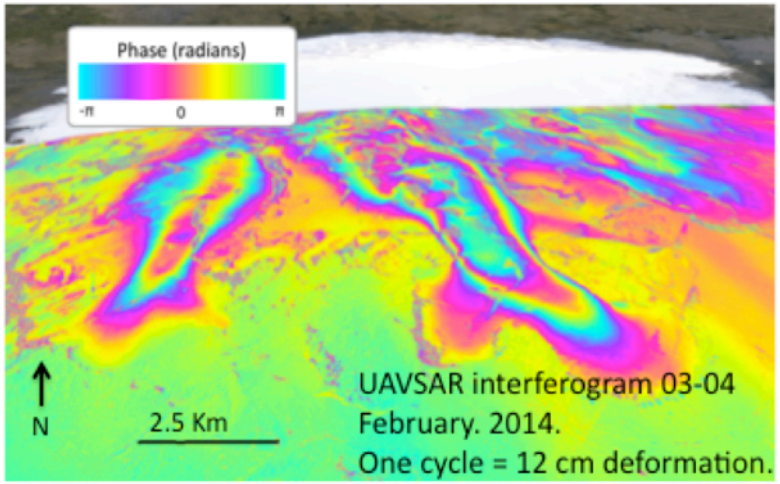

Hofsjokull glacier in Iceland

UAVSAR interferograms of East rift zone on Kilauea volcano, Hawaii.

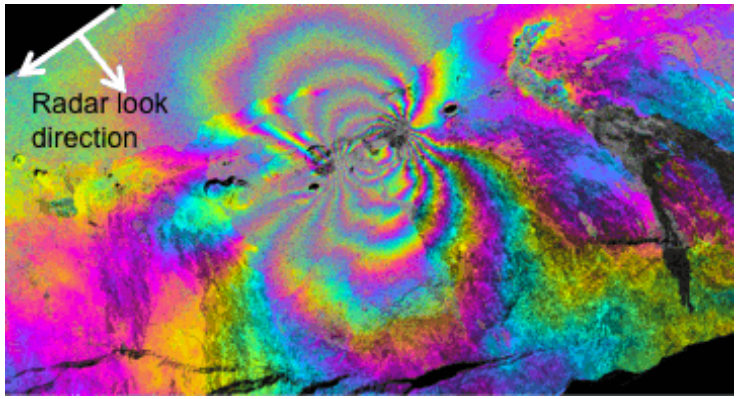

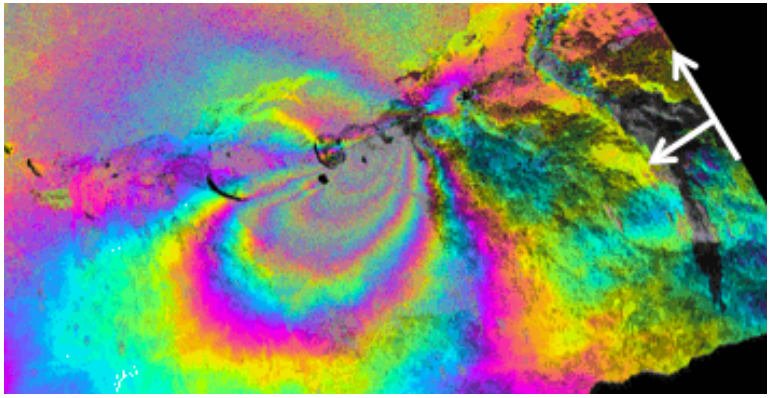

All images from NASA / JPL-Caltech

Limitation 1: Spatial coverage over slowly deforming areas

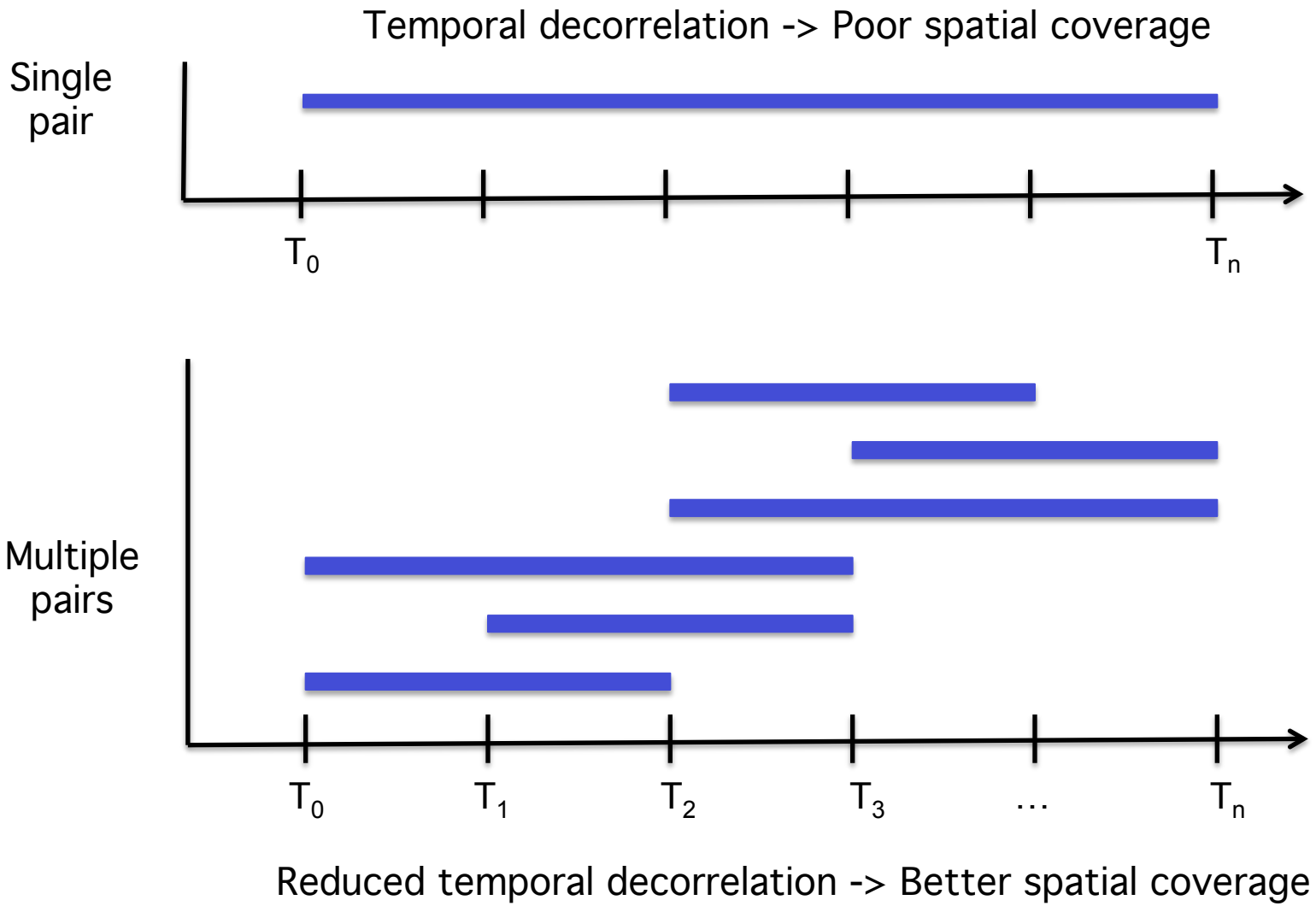

Limitation 2: Mitigating atmospheric and decorrelation noise

Example: Estimation of average LOS velocity

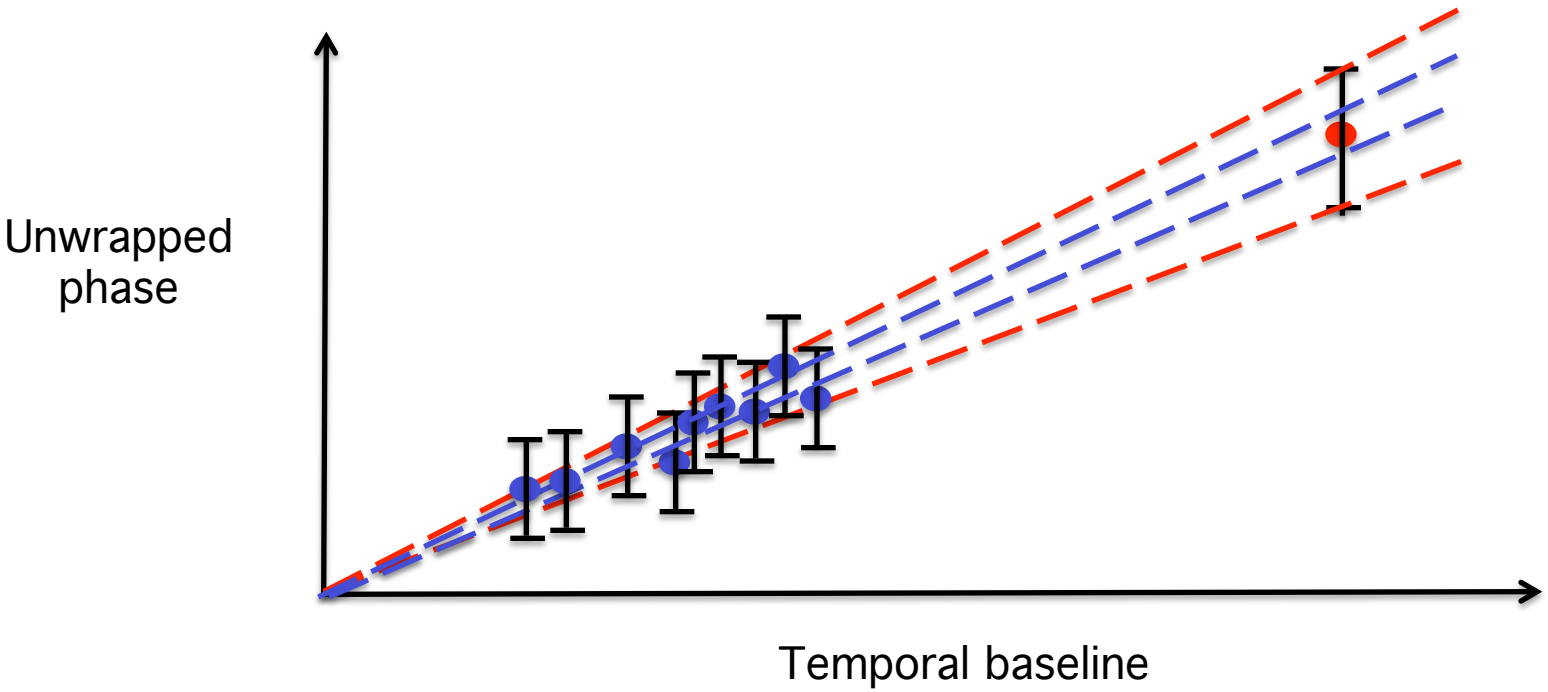

- Atmospheric contributions are uncorrelated in time (difference of > 1 day)
- We can beat down its contribution by combining information from multiple SAR acquisitions instead of just two.
- Decorrelation contributions and unwrapping errors are also less likely for more coherent interferograms.

Limitation 3: Detecting unwrapping errors

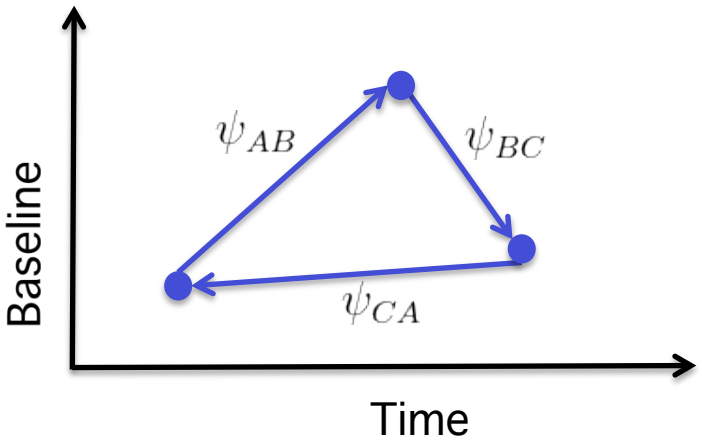

$$\left|\psi_{AB} + \psi_{BC} + \psi_{CA}\right| < \pi$$

Unwrapping errors can be detected by considering all possible closed loops in the interferogram network.

Image: Doin et al (2011)

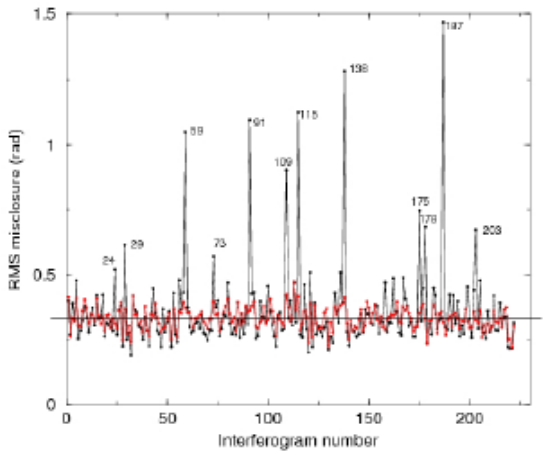

Figure 8. RMS misclosure for each interferogram (black without unwrapping error correction, red after automatic correction) to allow identification of unwrapping errors.

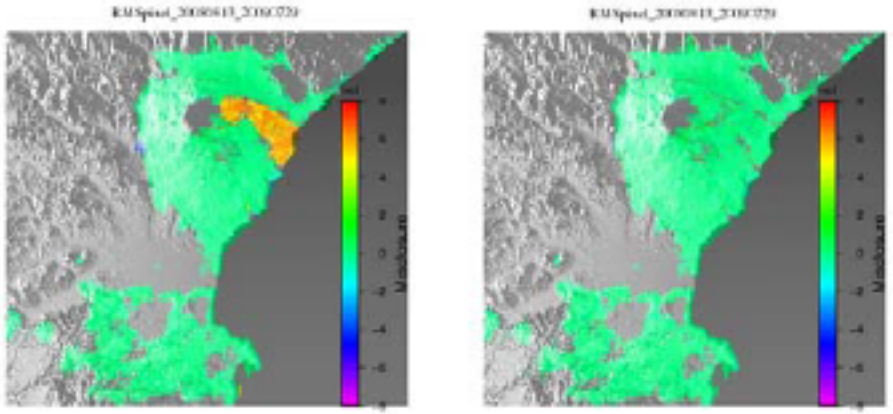

Figure 10. Interferometric misclosure maps for interferogram 187 before (left) and after (right) unwrapping error correction.

Limitation 4: DEM errors

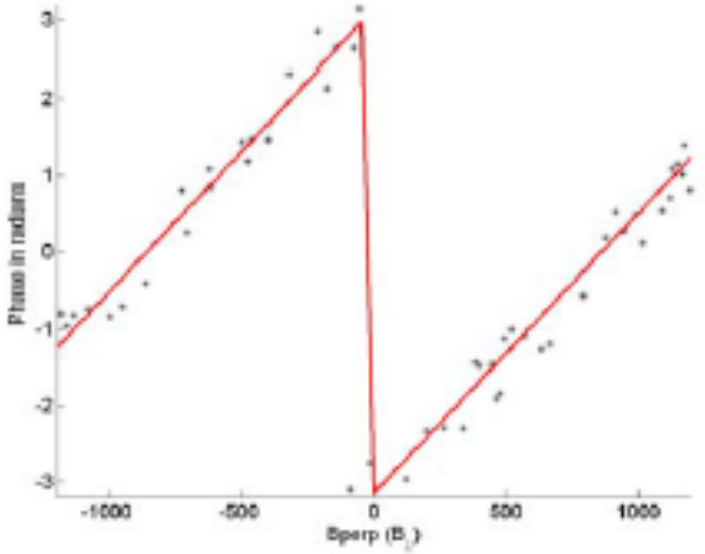

$$\phi_{dem} = \frac{4\pi}{\lambda} \cdot \frac{B_{\perp}}{r \cdot \sin\theta} \cdot \delta z$$

(Pixel phase – local average) vs Bperp

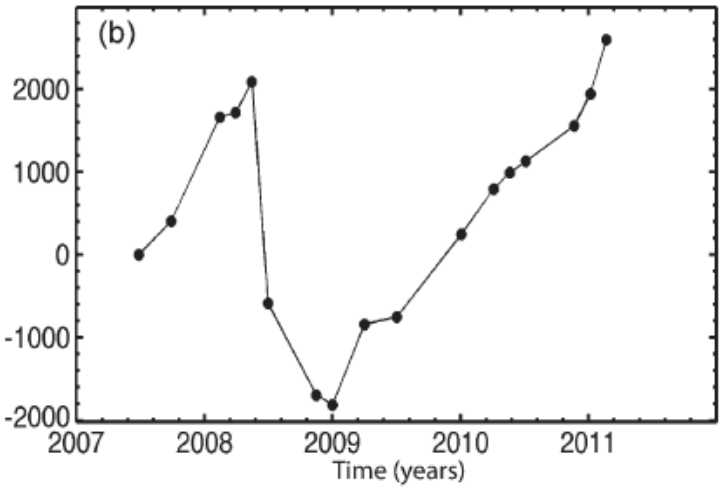

Image: Fattahi (2014)

Bperp vs Time for ALOS PALSAR

- (Pixel phase – local average) shows a trend w.r.t perpendicular baseline
- DEM error cannot be distinguished from deformation in the case of systematic orbit drift – ALOS PALSAR.

Motivation for Time-series InSAR

- Science argument:
  - Would time-history of surface deformation better inform the scientists about active geophysical phenomena over a given area?
  - Would time-history allow scientists to resolve or decouple contributions from different active phenomena based on associated time-scales?

- Overcoming the limitations of D-InSAR
  - Slowly deforming areas
  - Atmospheric artifacts
  - Unwrapping errors
  - DEM errors

Time-series InSAR techniques

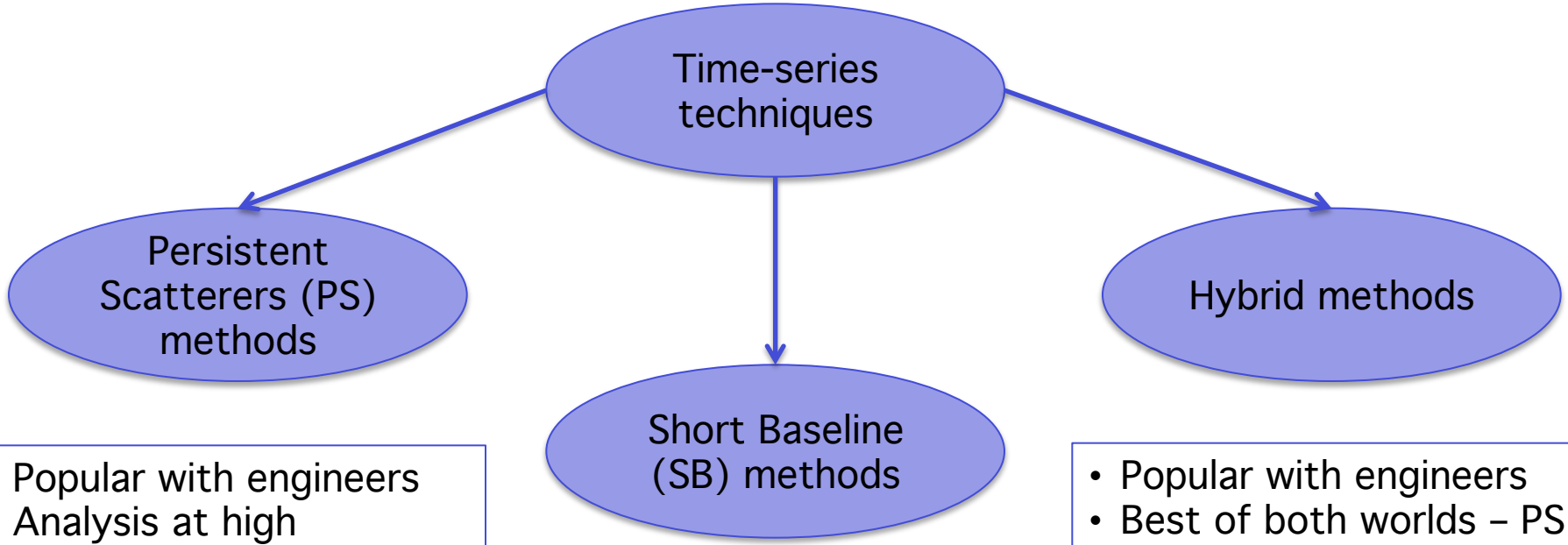

- Popular with engineers
- Analysis at high resolution - single look pixel scale.
- Computationally intensive.
- Typically used for small area analysis and infrastructure monitoring

- Popular with scientists
- Analysis at lower resolution - multi-look pixel scale.
- Typically used for large area analysis.

- Popular with engineers
- Best of both worlds – PS and SB
- Extension of PS techniques
- Newer approach and becoming more popular
- More robust approach

What are PS and DS?

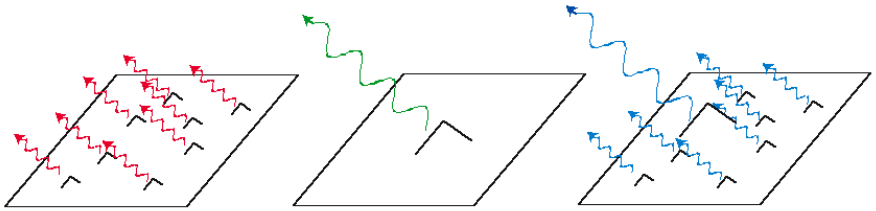

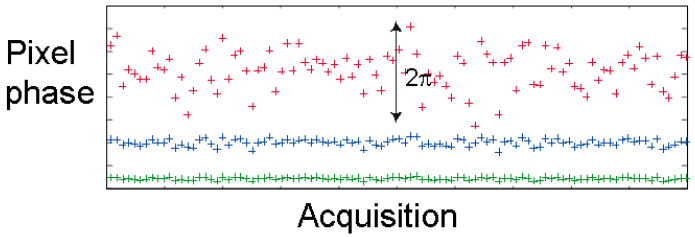

PS are corner reflector like resolution elements that are characterized by a dominant scatterer.

Use statistical techniques to identify scattering elements that do not change too much with time or geometric baseline.

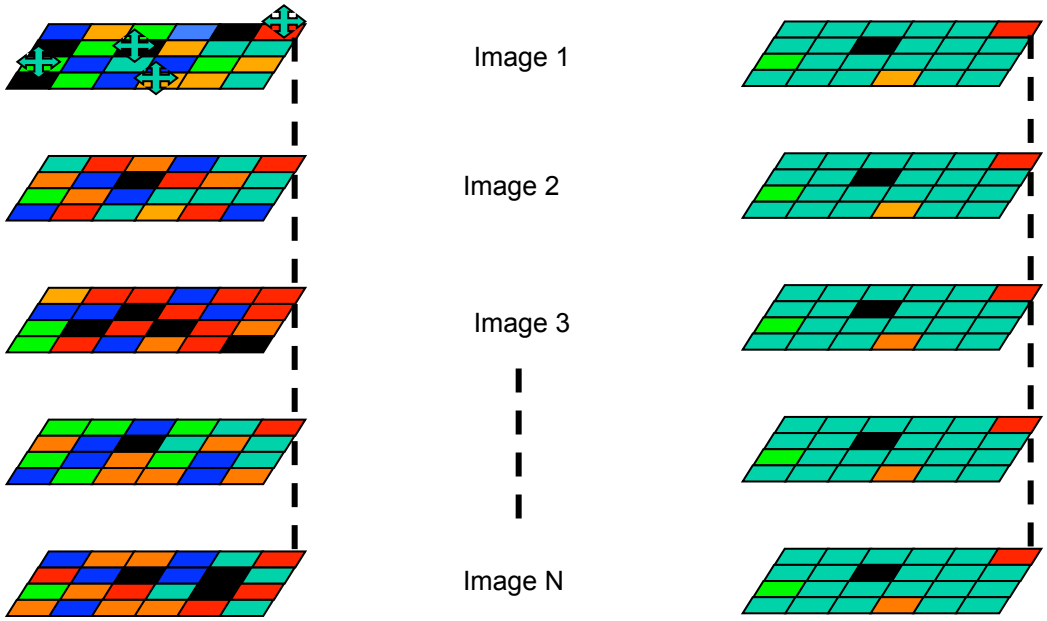

PS Interferogram network

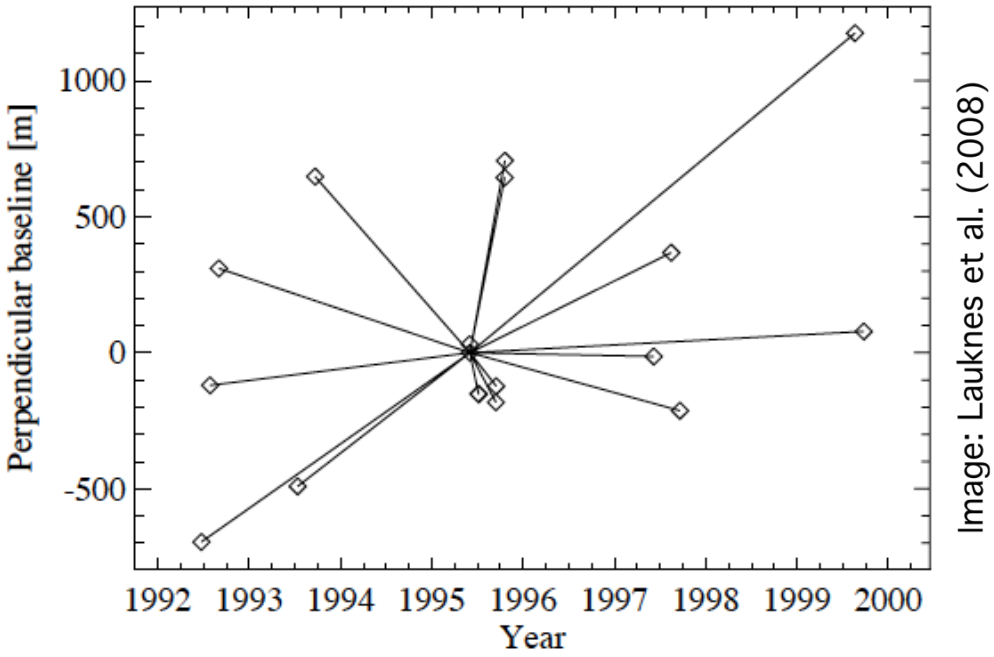

- Ideal point scatterers do not decorrelate with baseline.
- Common master network contains the same information as any other interferogram network.
- Master scene typically is located near the centroid in time-space and baseline space.

Amplitude-based PS identification

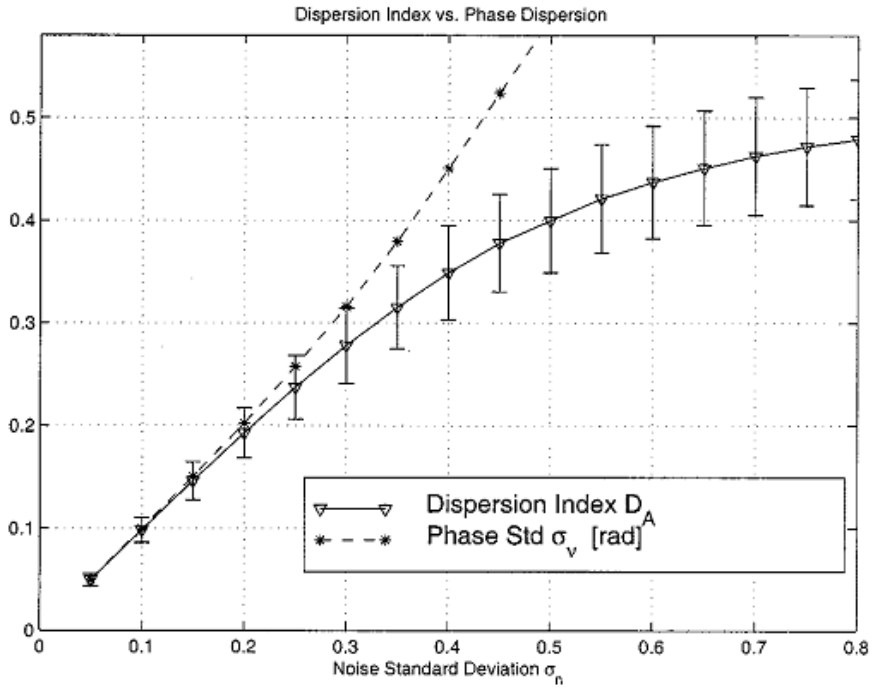

Image: Ferretti et al. (2000)

Simple signal model for observed SAR data.

$$s_i = 1 + n_i \qquad \forall i = 0, 1, \cdots, N$$

$$D_A = \frac{\sigma_{|s|}}{\mu_{|s|}}$$

$$\text{Amplitude Dispersion} = \frac{\text{Std. dev of amplitude}}{\text{Mean of amplitude}}$$

- Amplitude stability is used as a proxy for phase stability.
- Can be easily computed using a stack of coregistered SLCs.
- Works very well in urban areas.
- Can be tuned for different scattering models – e.g, two dominant scatterers etc.

Phase-based PS identification

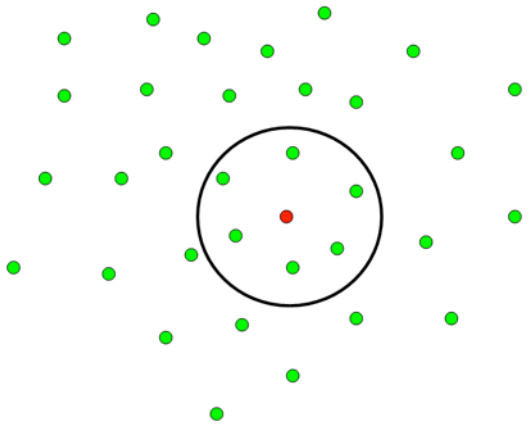

$$\phi_{ifg} = \phi_{defo} + \phi_{aps} + \phi_{orb} + \Delta\phi_{topo} + n$$

Deformation	Spatial ↓	Temporal ↓
Atmospheric phase screen	Spatial ↓	Temporal ↑
Precise orbit errors	Spatial ↓	Temporal ↑
Topo correction error	Spatial ↑	∝ Baseline
Uncorrelated noise terms	Spatial ↑	Temporal ↑

↑ High frequency ↓ Low Frequency

- StaMPS (Stanford Method for PS) framework by Andy Hooper
- Initialize network with reasonably stable pixels
  - Iteratively identify a self-consistent network of stable pixels
  - Weights of pixels based on phase stability
- Usually converges in about 7-8 iterations
- Performs better in natural terrain than amplitude-based methods.

Typical PS workflow

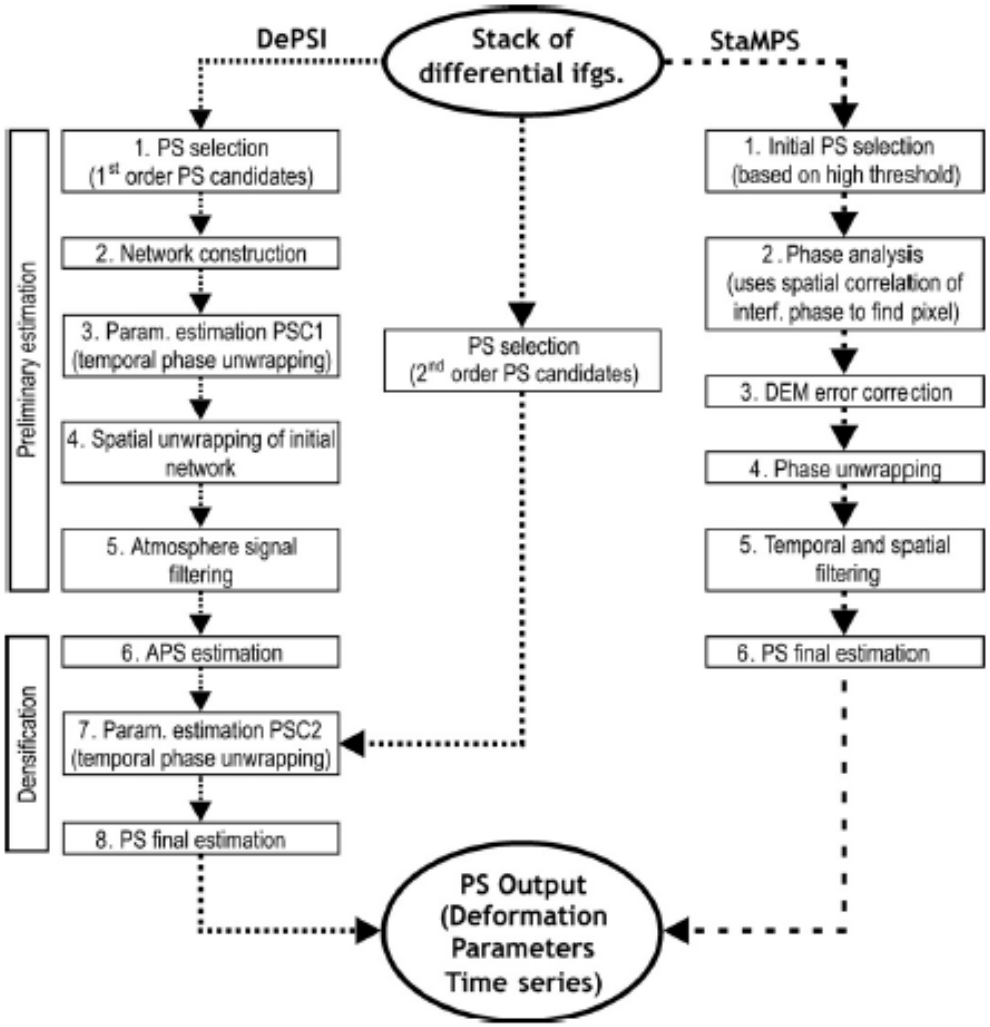

Fig. 3. DePSI and StaMPS comparative PS-InSAR flow diagram of the processing chain.

Image: Sousa et al. (2010)

- Coregistered stack of SLCs or differential ifgs is common to all PS implementations.
- Atmospheric signal is removed by temporal and spatial filtering.
- Quality of phase unwrapping depends on density of PS over area of interest.

PS - Phase unwrapping

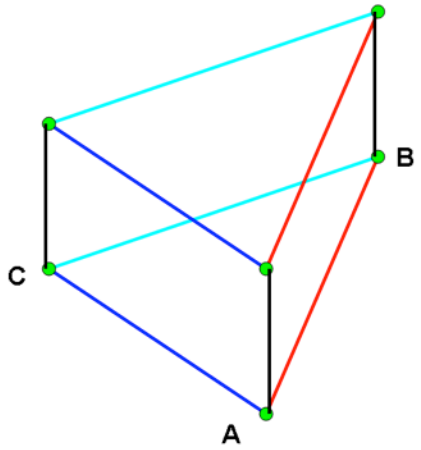

Unwrapping grid is Delaunay triangulation in spatial domain and regular grid in time domain.

Space first

- Unwrap each interferogram in space using conventional 2D techniques
- Unwrap each edge in time
- Adjust each unwrapped interferogram to accommodate changes.

Time first

- Unwrap each edge of Delaunay triangulation in time
- Use unwrapped solution as initial guess to spatial unwrapping using conventional 2D techniques.

Applications of PS

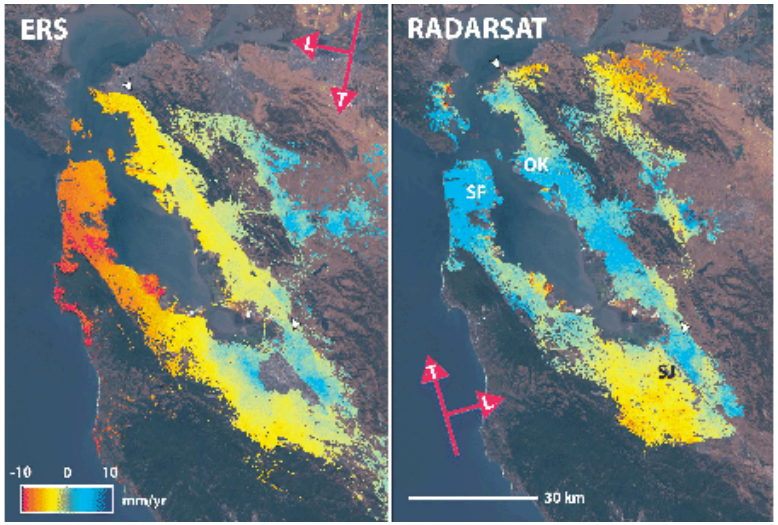

Fault activity in the San Francisco Bay Area (Image: TRE and UC Berkeley)

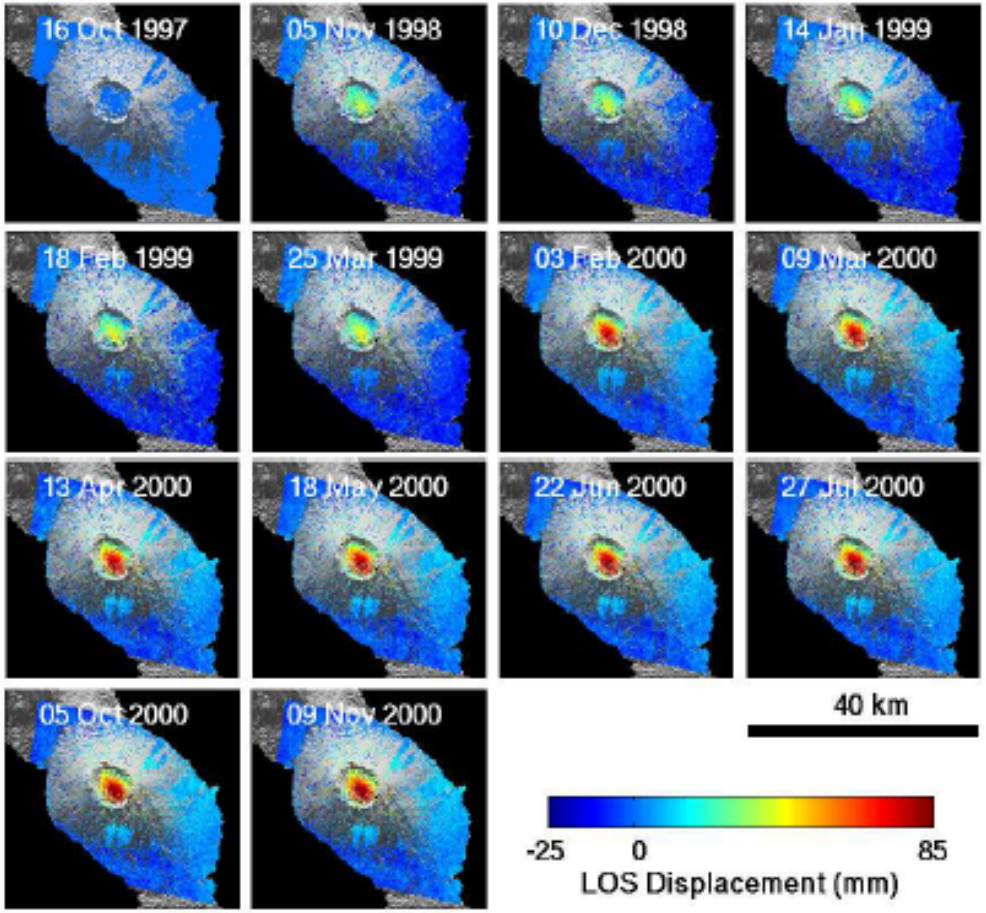

Deformation time-series for Volcan Alcedo in the Galapagos using ERS-data (Image: Andy Hooper)

Building-scale monitoring

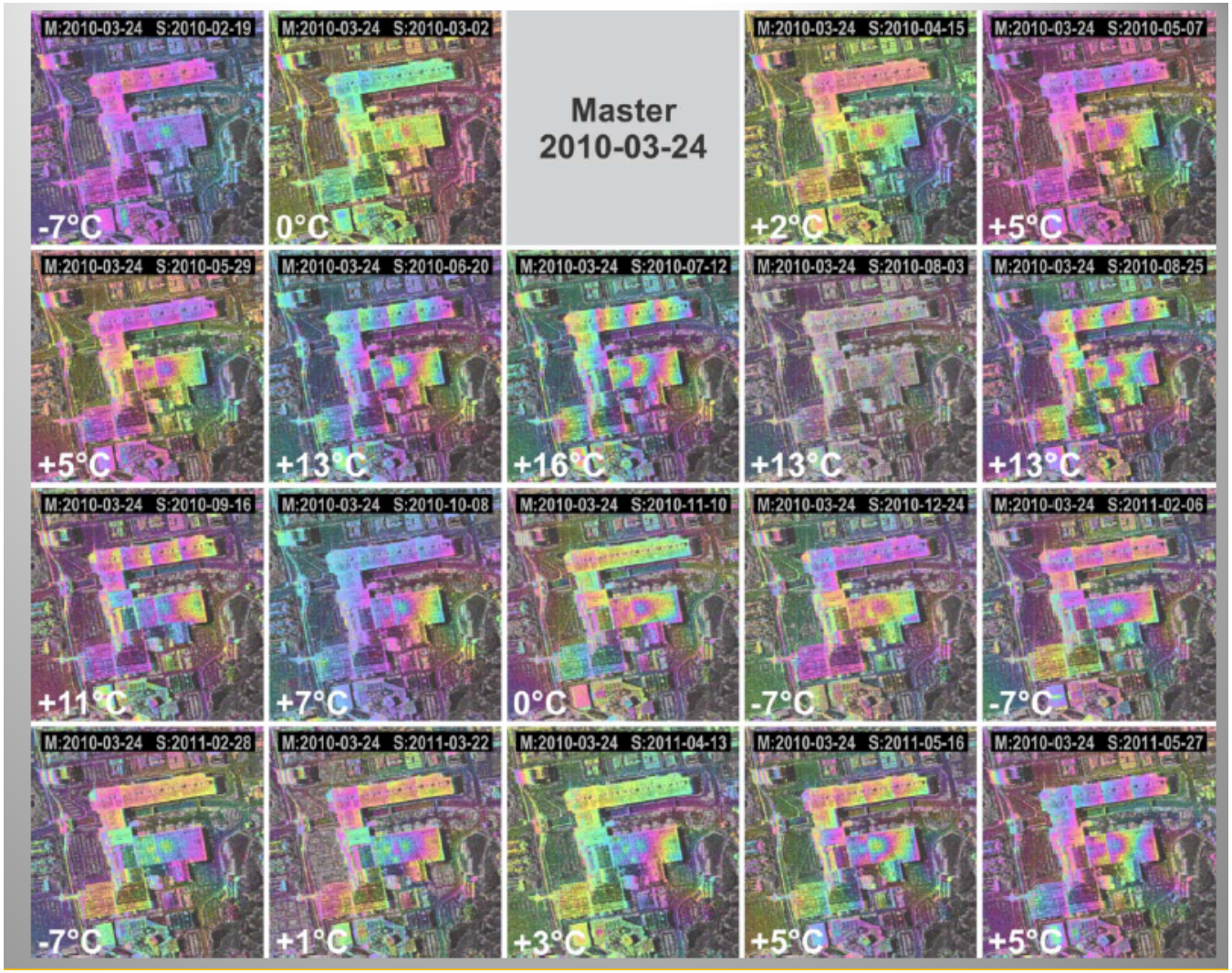

Image: Jendryke et al (2013)

Effect of resolution on PS

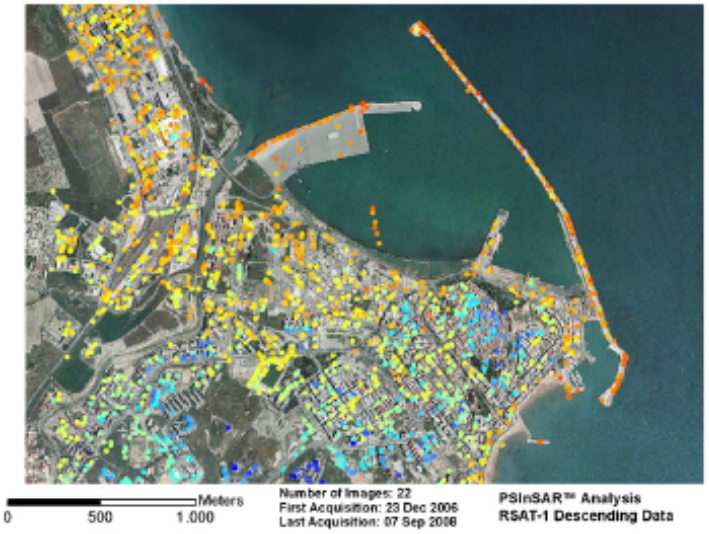

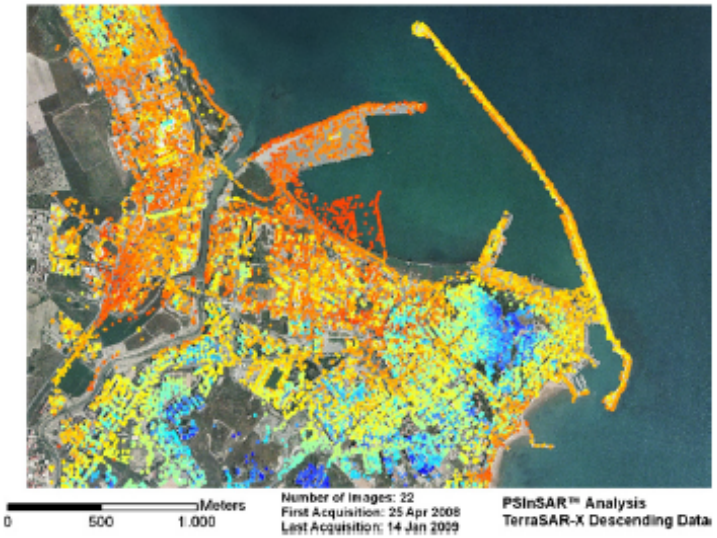

Image: TRE (2010)

- Theory: Higher resolution leads to fewer mixed pixels and hence, higher PS density.
- This has been validated by recent high resolution sensors – TSX, CSK, RSAT2.
- High resolution acquisitions resulted in significantly higher PS density than from older C-band sensors – ERS, Envisat and Radarsat-1.

Short Baseline Subset (SBAS) method

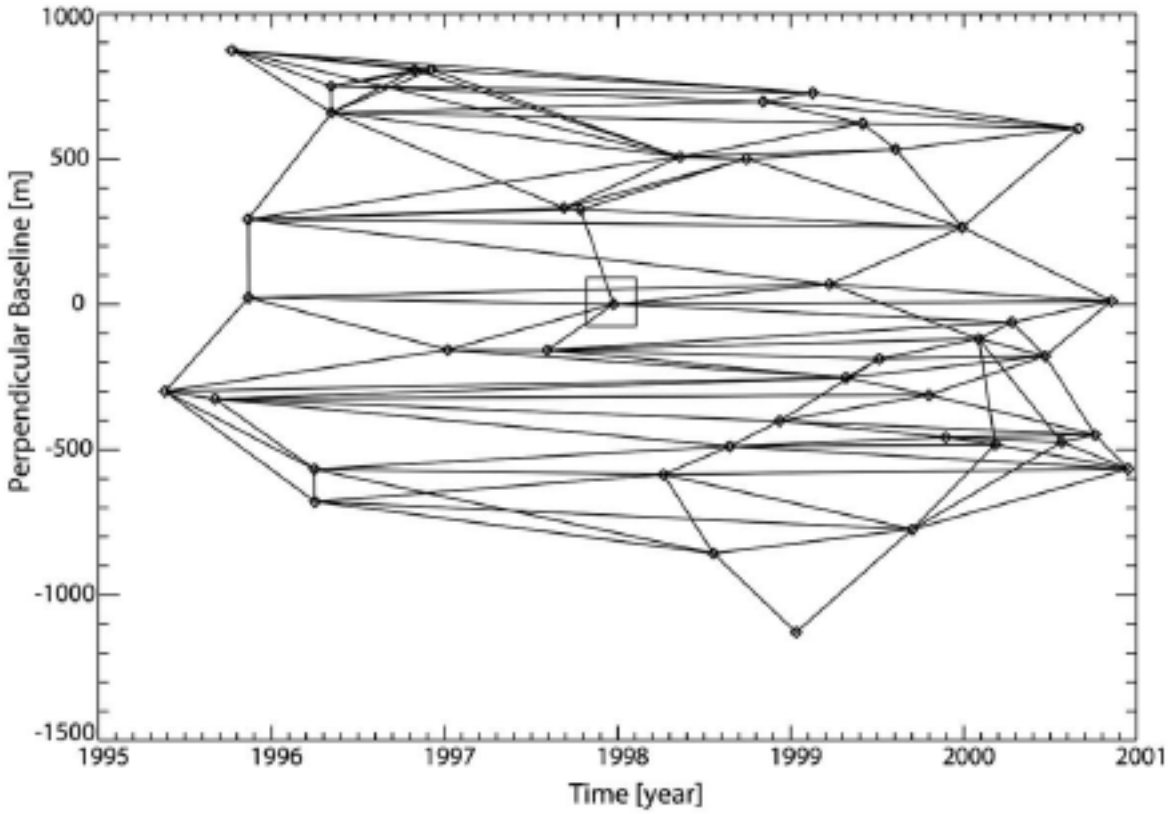

Time-baseline plot for San Francisco ERS dataset
(Agram et al., 2011)

Simple formulation

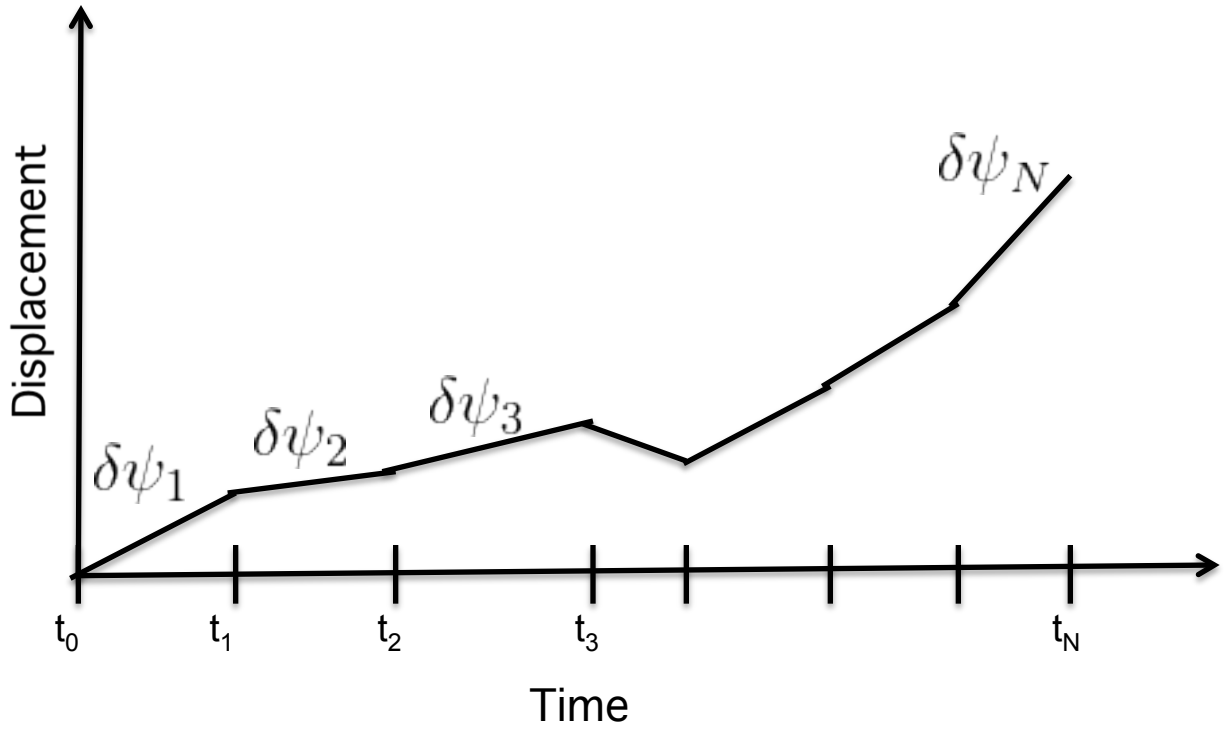

$$\psi(t_N) = \sum_{i=1}^{N} \delta\psi_i$$

Estimated time-series is sum of piece-wise terms

$$\psi_{ifg}(t_i, t_j) = \sum_{k=i}^{j} \delta\psi_k$$

Interferometric unwrapped phase is sum of piece-wise terms spanned by the acquisitions

Variants of SBAS

- Original SBAS implementation (Berardino et al., 2002) demanded similar amount of rigor in coregistration as PS methods.

- Modifications can be easily implemented
  - Reuse of already existing D-InSAR tools
  - Heavy filtering of interferograms reduces resolution and relaxes strict coregistration requirements
  - Simpler workflow

- Most modifications at the inversion stage
  - Inversion of wavelet coefficients / data
  - Use of GPS-like model including seasonal terms, step functions, polynomials etc

- Example: NSBAS, MInTS etc.

Typical SBAS workflow

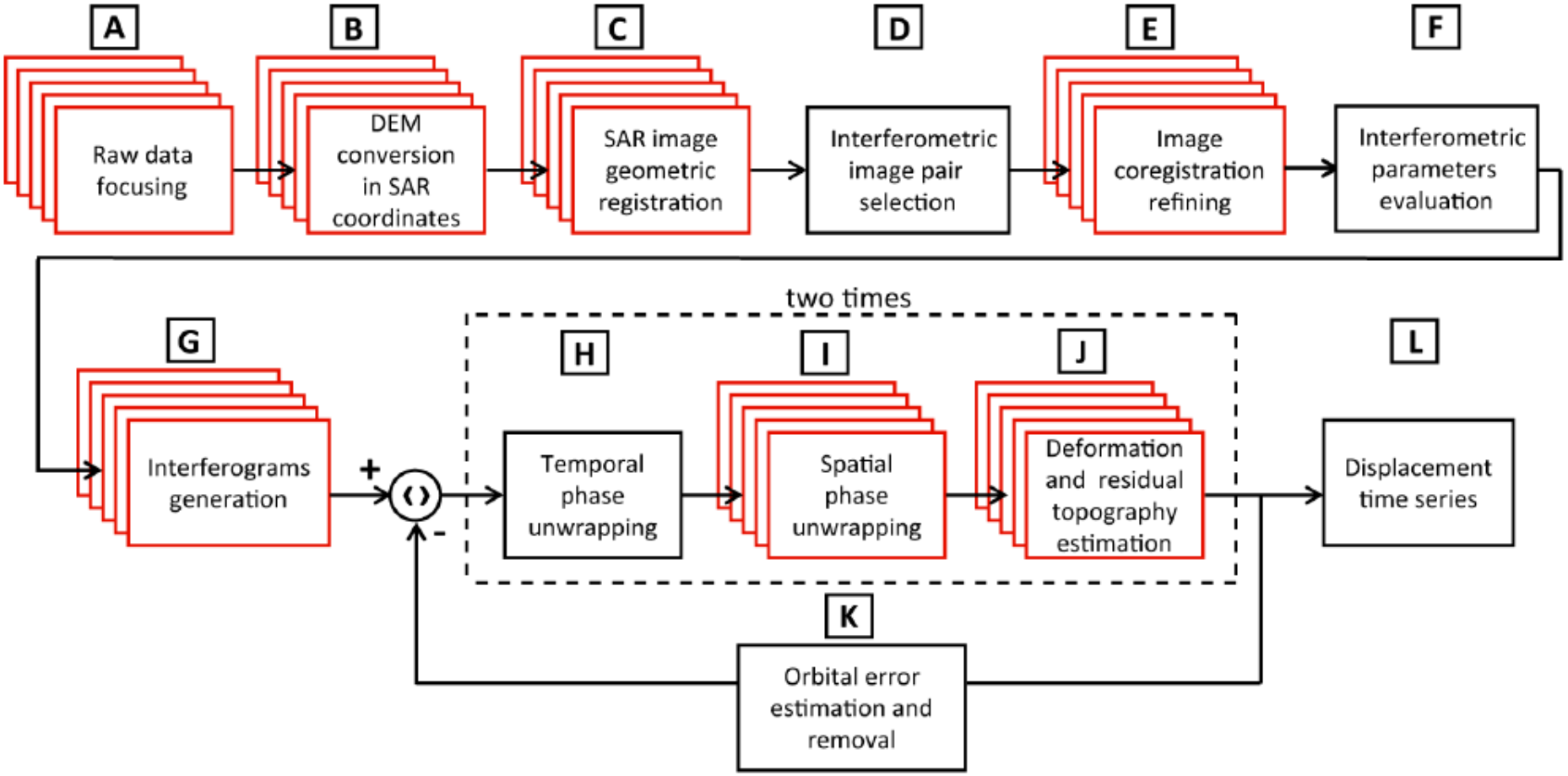

Image: P-SBAS workflow. Zinno et al. (2014)

Hybrid time-series methods

- Best of both worlds.
  - SqueeSAR™ approach (Ferretti, 2011)

- Adaptive feature preserving multilooking
  - PS at full resolution
  - DS multi-looked based on similar neighbors.
  - SBAS-like approach for DS inversion

- Resolution of time-series product depends on location.

- Neighbors typically identified by comparing SAR amplitude distributions.

- By design, an extension of PS techniques and relies heavily on precise coregistration
  - Computationally intensive

Multi-looking with self-similar neighbors

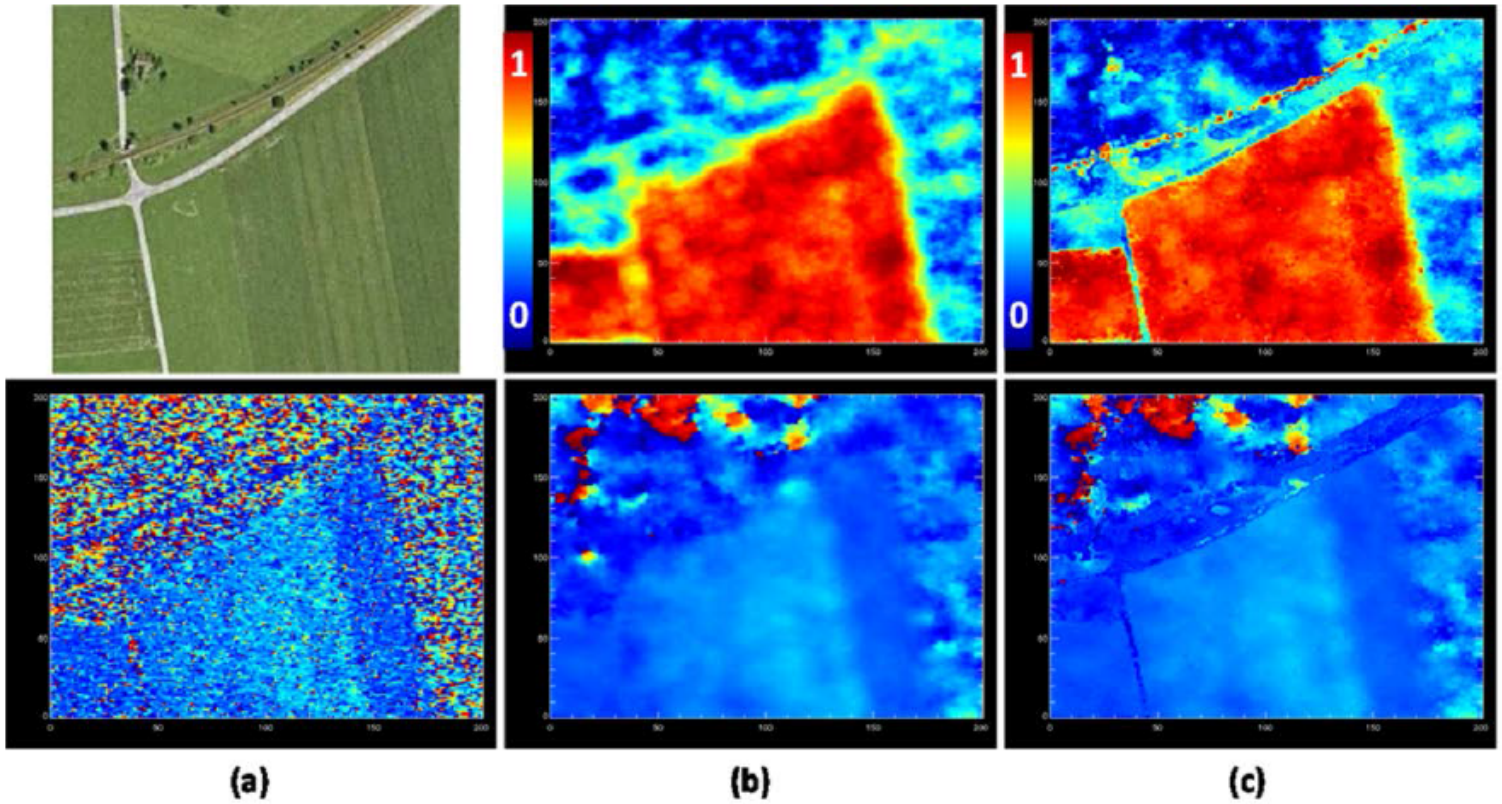

Figure 18: (a) is a Google Earth image and its single-look interferogram. (b) is coherence and interferogram estimate after boxcar multi-looking. (c) is coherence and interferogram estimate after adaptive spatial filtering.

Image: Goel and Adam (2012)

Distribution of PS vs DS

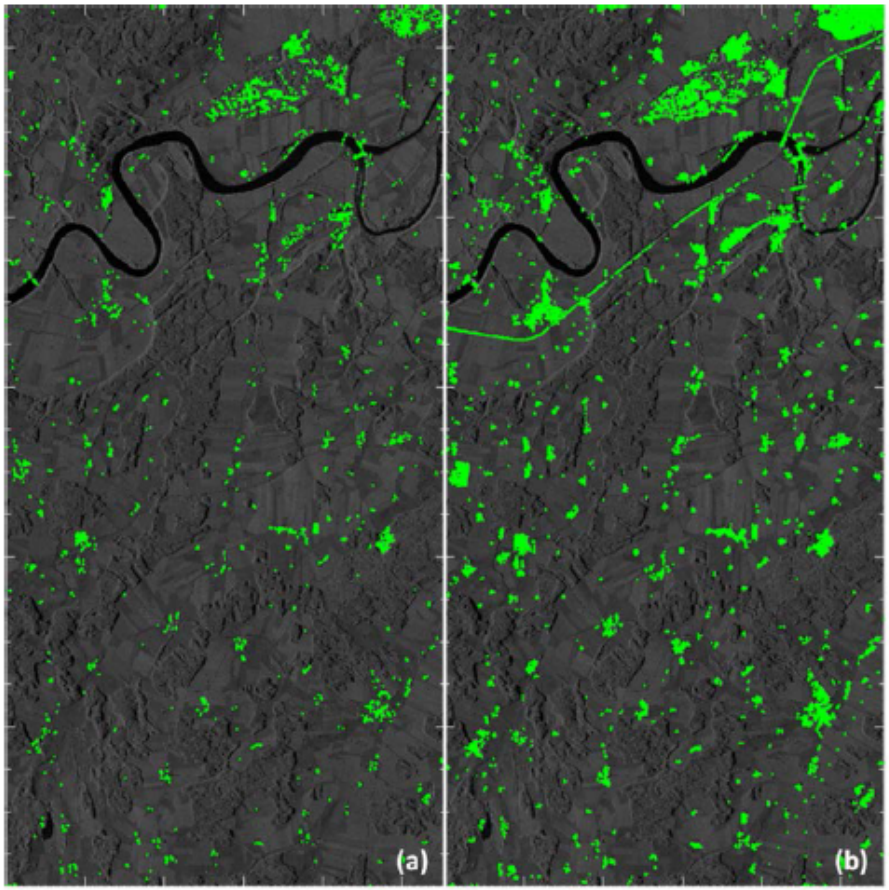

Figure 22: TerraSAR-X image of the gas storage site in Germany. (a) shows the PSs in green (54,258 points), whereas (b) shows the PSs and DSs in green (284,081 points). The density of PSs is very low compared to the DSs in this non-urban area.

Image: Goel (2013)

Another example

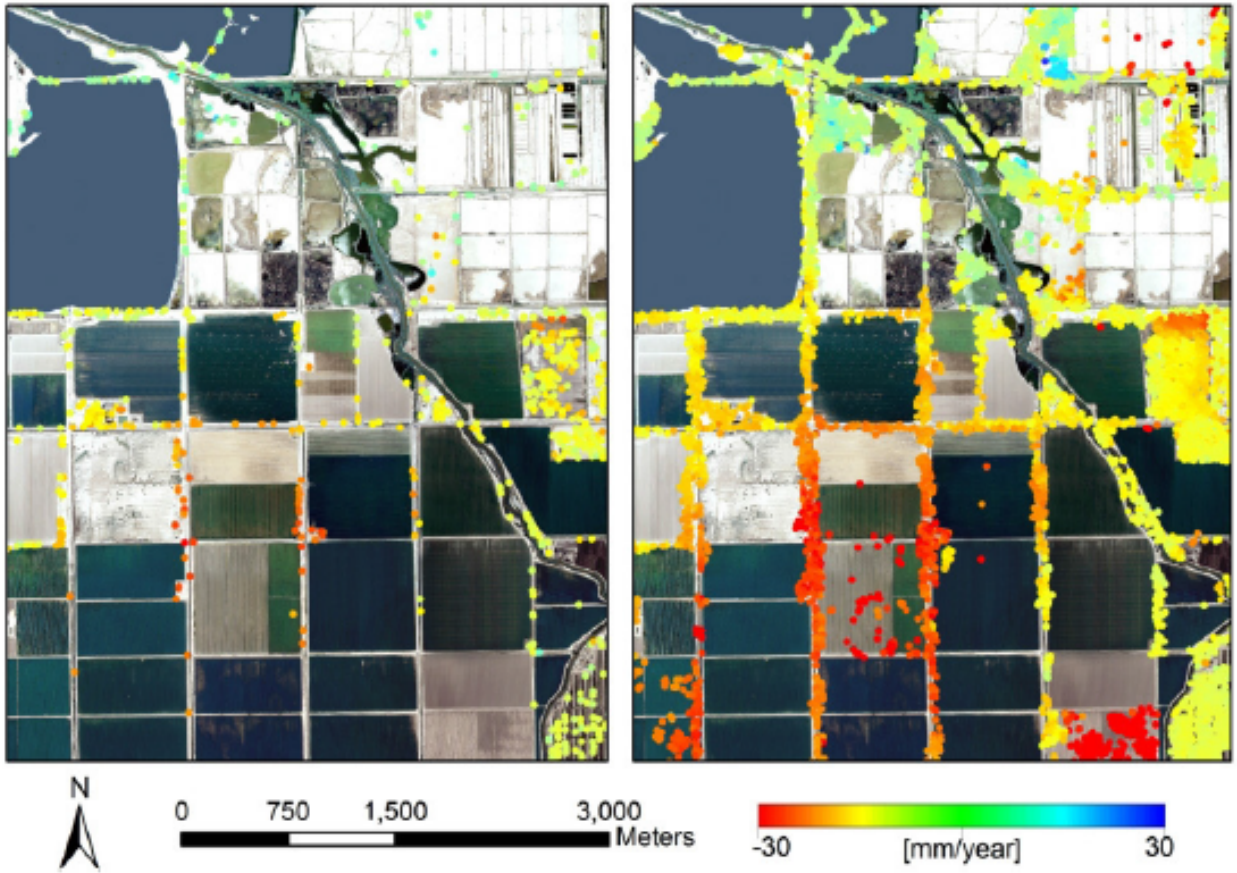

Figure 3. PSInSAR™ (left) and SqueeSAR™ (right) LOS displacement results identified from the Radarsat-1 descending dataset for a subsection of the Salton Sea geothermal field. Total displacement measured over the entire time period analyzed (2006 to 2008) ranged from -62 mm (representing movement away from the satellite) to 28 mm (movement towards the satellite).

Image: TRE (2011)

Challenges for time-series InSAR

- Phase unwrapping
  - Particularly for high resolution analysis
- Troposphere
- Mission continuity
  - Longer time-series needed to discriminate between different geophysical phenomena
- Multi-dimensional time-series by combining stacks from different geometries
- Computational and storage needs
- Uncertainty products
  - Time-series uncertainties not typically reported